Macondo Oil in Deep-Sea Sediments: Part 1 – Sub-sea Weathering of Oil Deposited on the Seafloor

Scott A. Stout[1*] and James R. Payne[2]

[1]NewFields Environmental Forensics Practice, LLC, 300 Ledgewood Pl., Suite 305, Rockland, MA
[2]Payne Environmental Consultants, Inc., 1651 Linda Sue Ln., Encinitas, CA

Abstract

Chemical analysis of sediment cores collected up to 8 km from the Macondo well in 2010/2011 demonstrate the extent of weathering of the Macondo oil deposited in deep-sea sediments. On average, dissolution and biodegradation of the oil on the seafloor increased with distance from the well indicating weathering occurred rapidly and overwhelmingly during the oil's transport as dispersed oil droplets within the deep-sea plume. Beyond about 5 km from the well, the oil deposited on the seafloor had lost most mass below C_{25}, was relatively enriched in *n*-C_{25}+ *n*-alkanes and C_3- and C_4-alkylated benz[*a*]anthracenes/chrysenes, the latter owing to 95% depletion of total PAHs. Biodegradation of C_{28} and C_{29} tricyclic terpanes, C_{34} and C_{35} 17α(H),21β(H)-homohopanes, C_{27} 13β(H),17α(H)-dia and C_{27} 14β(H),17β(H)- steranes and dissolution of C_{26} to C_{28} triaromatic steroids occurred. The results provide a means to distinguish Macondo oil in deep-sea sediments from naturally-occurring seep oils and pervasive ambient background hydrocarbons.

Keywords

Deepwater Horizon
Dissolution
Biodegradation
Biomarkers
PAH
Deep-sea plume

*corresponding author: Tel.: +1 781 681 5040; e-mail: sstout@newfields.com

1. Introduction

Crude oil released in the Gulf of Mexico (April 20 to July 15, 2010) from the failed Macondo well at a water depth of ~1500 m following the explosion of the *Deepwater Horizon* (DWH) drill rig experienced a range of environmental fates. Buoyancy forces caused larger droplets of oil to be transported (roughly) vertically through the water column to the sea surface where it formed surface slicks, mousses, and sheens that were spread widely by wind and currents over vast areas of the northern Gulf of Mexico (GoM) during the 87-day spill, before finally dissipating five weeks after the well was capped on July 15 (Ramseur, 2010). Numerous studies showed that most of the surfaced oil (i.e., oil not subjected to *in-situ* burning, chemical dispersion, or mechanical recovery) experienced the typical progression in weathering that predictably altered the chemical and physical properties of the oil (Aeppli et al., 2012, 2014; Liu et al., 2012; Carmichael et al., 2012; Kiruri et al., 2013; Hall et al., 2013; McKenna et al., 2013; Lewan et al., 2014; Ruddy et al., 2014; Daling et al., 2014; Faksness et al., 2015; Stout et al., 2016). These studies collectively showed that surfaced oil experienced up to 20-25% losses to dissolution of <C8 aliphatics and aromatics during its ascent, with increasing effects of evaporation, continued dissolution, and/or photo-oxidation upon reaching the surface. Biodegradation of surface slicks progressed more slowly -- only affecting surfaced oil that stranded along shorelines.

Another fraction of the crude oil released from the failed Macondo well remained within the deep-sea. This subsea oil existed as physically- or chemically-dispersed, neutrally buoyant oil droplets (< 50 μm; Lindo-Atichati et al., 2014) that formed as the oil (and gas) was ejected under high pressure and turbulent conditions at the wellhead. The physical atomization of the oil was enhanced or (at least) retained by chemical dispersant injected into the emerging plume (Socolofsky et al., 2011; 2015). The dispersed oil droplets diffused and were advected horizontally within an extensive deep-sea intrusion layer, or "plume", that formed ~200 to 500 m above the wellhead at a water depth of ~1000 to 1300 m (e.g., Camilli et al. 2010; Socolofsky et al., 2011; Atlas and Hazen, 2011; Ryerson et al., 2012; Payne and Driskell, 2015a). Deep water column studies tracked the plume in multiple directions (e.g., Spier et al., 2013; Boehm et al., 2016), but mostly toward the southwest where oil droplets were still recognized ~155 km from the well (Payne and Driskell, 2015a).

Oil droplets within the deep-sea plume did not experience the same types of weathering as was experienced by the surfaced oil because evaporation or photo-oxidation could not affect the subsea oil. However, dissolution and biodegradation undoubtedly altered the subsea oil droplets, the rates of both processes likely accelerated by the small droplet size (i.e., large surface area-to-volume ratio) of the dispersed oil particles within the deep-sea plume (Prince et al. 2013; Driskell and Payne, submitted).

Dissolution of oil within the deep-sea plume is evident from numerous studies that observed elevated concentrations of hydrocarbons in water samples collected between 1000 and 1300 m during or shortly after the spill. These studies measured elevated concentrations of BTEX (Hazen et al., 2010), PAHs (Diercks et al., 2010; Boehm et al., 2016), or numerous alkane and aromatic totals (Spier et al., 2013), although none specifically distinguished between hydrocarbons in a dissolved versus particulate phase. Clear evidence that dissolution affected the dispersed oil was obtained through the study of large volume water samples filtered at sea in which the dissolved (<0.7 μm) and particulate phases were analyzed separately using the method of Payne et al. (1999). Specifically, results for paired samples collected from deep-sea plume waters often revealed dissolved and particulate phases that were enriched and depleted, respectively, in the more soluble hydrocarbons (Payne and Driskell, 2015a).

Evidence for biodegradation in the deep-sea plume also exists, and was not unexpected given the presence of indigenous oil-degrading heterotrophic microbes in the deep-sea due to the existence of natural gas and oil seeps throughout the region. Increased microbial cell densities and a widely observed dissolved oxygen (DO) deficit within the deep-sea plume (Hazen et al., 2010) showed that the indigenous deep-sea microbes rapidly responded and completely respired the dissolved gases and partially respired the dispersed oil (Valentine et al., 2010; Kessler et al., 2011).

The extent(s) to which dissolution and biodegradation affected the dispersed oil within the deep-sea was only partially represented by the many thousands of water column samples collected from the plume during the spill. This is because quantifying the effects of dissolution and biodegradation of discrete oil droplets within the deep-sea plume was hampered by the difficulty of physically sampling the highly-diluted oil droplets in field-collected grab samples from the water column. However, through multiple mechanisms summarized in the accompanying study (Stout et al., submitted) at least some of the dispersed oil droplets from the deep-sea plume(s) were deposited on

the seafloor within an “oily floc,” where they accumulated and could be more practically sampled.

In the present study, we present results that demonstrate the range to which dissolution and biodegradation affected the Macondo oil present on the seafloor in 2010/2011. We accomplish this by focusing on results obtained from sediment cores collected up to 8 km (5 miles) from the well, which were carefully collected to retain any “oily floc” associated with Macondo oil deposition. The results show that the Macondo oil in deep-sea sediment was dramatically and, on average, progressively weathered with increasing distance from the well up until about 5 to 8 km from well. This indicates (1) the weathering occurred rapidly and overwhelmingly during the oil’s transport within the deep-sea plume (and not after its deposition) and (2) after about 8 km of transport the oil droplets in the plume were so severely weathered that the oil carried and deposited in sediments beyond 8 km from the well were universally, severely weathered. Results indicate the physical and chemical dispersion of the oil near the wellhead indeed allowed for dissolution and biodegradation to progress rapidly – but only to a point after which a wax-rich, severely weathered Macondo oil residue with a highly consistent “fingerprint” remained to be deposited in sediments at further distances from the well. The accompanying study (Stout et al., submitted) uses knowledge gained herein to define the lateral and vertical extent of the “fingerprintable” Macondo oil beyond 8 km from the well with special emphasis on distinguishing it from pervasive background hydrocarbons and localized impacts of oil from the area’s natural oil seeps.

2. Samples and Methods

2.1 Sediments

Table 1 lists the 15 surveys/cruises from which a total of 2782 sediment samples from 729 cores were collected in 2010/2011 (Fig. 1). All of the sediment samples collected were included either in this study or Stout et al. (submitted). In this study, we focus on cores collected within 8 km (5 miles) of the wellhead (Fig. 1) as these best demonstrate the weathering experienced by the Macondo oil that had accumulated on the seafloor. These cores were collected in four of the cruises indicated, *viz.*, HOS Davis 05, HOS Sweetwater 02 Leg 2, Sarah Bordelon 09, and HOS Sweetwater 6 Leg 1.

Cores considered to be higher resolution were those in which surface sediments were collected in 0 to 0.5, 0 to 1, 0 to 1.5, or 0 to 2 cm intervals. These cores contained between two and seven individual depth intervals that were isolated for study onboard each vessel, which provided a means to compare hydrocarbon profiles within the cores.

Notably, 47 lower resolution cores were collected early in the NRDA assessment during the cruises by the *Nancy Foster*, *Cape Hatteras,* and *Ron Brown* in 2010. As these cores' data became available it was evident that they provided too low a resolution (0-3, 0-5 and 0-10 cm) to unequivocally recognize the impact of the Macondo oil to the surface sediment due to the diluting effect of analyzing broader depth intervals. As the need for higher resolution cores was realized, all sediment cores from subsequent NRDA cruises were collected (1) with caution to preserve and collect any floc layer (see Payne and Driskell, 2015b) and (2) carefully processed at sea shortly after collection to obtain 0 to 0.5, 0 to 1, 0 to 1.5, or 0 to 2 cm intervals for chemical analysis, which allowed better recognition of any impact of Macondo oil to sediments (Table 1).

Additional deep-sea sediment cores collected in September and October 2010 during the response effort (OSAT-1, 2010) were originally evaluated but were also excluded from our assessment. Response cores collected within about 3 km of the wellhead indeed showed the presence of Macondo oil (and synthetic based mud), a conclusion also reached by OSAT-1 (2010). However, cores collected beyond this distance were equivocal with respect to the presence of Macondo oil. This result was attributed to (1) the difficulty of collecting any oily floc that may have been present (e.g., not retained due to bow wake of the sediment samplers) and (2) the relatively low resolution of the cores, wherein the 0-3 cm intervals were homogenized and analyzed, potentially diluting any oily floc in the uppermost core. Both of these shortcomings were explicable at the time these cores were collected because the pervasive existence of the oily floc on the seafloor was not yet recognized.

2.2 Sample Preparation

Sediment samples were carefully isolated from cores onboard shortly after collection. Individual core intervals for chemical analysis were placed in glass jars and frozen prior to being shipped cold to Alpha Analytical (Mansfield, Massachusetts) under full chain-of-

custody procedures. Upon receipt at the laboratory all samples were stored in the dark and frozen (-20ºC) prior to sample preparation and instrumental analysis.

Sediment samples (~30 g wet) were spiked with recovery internal surrogates (RIS; 5α-androstane, acenaphthene-d_{10}, chrysene-d_{12}), dried with anhydrous $NaSO_4$ and serially-extracted (3-times; 6, 2, and 0.5 hrs) using 100 mL fresh dichloromethane (DCM) on a shaker table. The extracts were combined, filtered through glass wool, dried with anhydrous Na_2SO_4, concentrated to 1 mL using Kuderna Danish apparatus and nitrogen blow-down, treated with activated copper to remove sulfur, and silica gel-cleaned using EPA Method 3630C, re-concentrated to 1 mL (as above) and spiked with surrogate internal standards (SIS; *o*-terphenyl, n-tetracosane-d_{50}, 2-methylnaphthalene-d_{10}, pyrene-d_{10}, benzo(b)fluoranthene-d_{12}, and 5β(H)-cholane) prior to instrument analysis. Each analytical batch of authentic samples (n<20) included a procedural blank (PB; 1 mL of DCM), a laboratory control sample (LCS) and LCS duplicate (LCSD), each consisting of 1 mL of DCM spiked with selected hydrocarbons in known concentrations to monitor method accuracy, the NIST 1582 crude oil standard reference material, and one sample duplicate (i.e., a single sediment prepared twice) as a measure of precision and reproducibility of the data.

2.3 Instrument Analysis

All sample extracts were analyzed using a (1) modified EPA Method 8015B and (2) modified EPA Method 8270 as described in the following paragraphs. Additional details of these methods are described elsewhere (Douglas et al., 2015).

Modified EPA Method 8015B was conducted via gas chromatography-flame ionization detection (GC-FID; Agilent 6890) equipped with a Restek Rtx-5 (60m x 0.25 mm ID, 0.25 μm film) fused silica capillary column. Extracts were injected (1 μL, pulsed splitless) into the GC programmed from 40°C (1 min) and ramped at 6°C/min to 315°C (30 min) using H_2 (~3 mL/min) as the carrier gas. This analysis was used to determine the concentrations of GC-amenable total petroleum hydrocarbons (TPH; C_9-C_{40}) and individual *n*-alkanes (C_9-C_{40}) and (C_{15}-C_{20}) acyclic isoprenoids (Table S-1). Prior to sample analysis a minimum five-point calibration was performed to demonstrate the linear range of the analysis. The calibration solution was composed of selected aliphatic hydrocarbons within the *n*-C_9 to *n*-C_{40} range. Analyte concentrations in the standard

solutions ranged from 1 ng/μL to 200 ng/μL. Target analytes that were not in the calibration solution had the average response factor (RF) of the nearest eluting compound(s) assigned as follows: RF of *n*-C_{14} assigned to C_{15} isoprenoids, *n*-C_{15} assigned to C_{16} isoprenoids; *n*-C_{17} assigned to nor-pristane, and *n*-C_{40} assigned to *n*-C_{39}. All calibration solution compounds that fall within the window were used to generate the average RF for TPH. TPH was quantified by integrating the total C_9-C_{40} area after blank subtraction. Calibration check standards representative of the mid-level of the initial calibration and the PB were analyzed every 10 samples. The check standard's response was compared versus the average RF of the respective analytes contained in the initial calibration. All authentic samples and quality control samples were bracketed by passing mid-check standards.

Modified EPA Method 8270 was conducted via gas chromatography-mass spectrometry (GC-MS; Agilent 7890 GC with 5975c MS) with the MS operated in the selected ion monitoring (SIM) mode for improved sensitivity. Extracts were injected (1 μL, pulsed splitless) into the GC containing a 60m x 0.25 mm ID, 0.25 μm film, Phenomenex ZB-5 capillary column and the oven programmed from 35°C (1 min) and ramped at 6°C/min to 315°C (30 min) using He as the carrier gas. This analysis was used to determine the concentrations of 62 parent and alkylated decalins, polycyclic aromatic hydrocarbons (PAH), sulfur-containing aromatics, and 54 petroleum biomarkers (i.e., tricyclic and pentacyclic triterpanes and steranes, and triaromatic steroids (Table S-1). Prior to sample analysis, the GC-MS was tuned with perfluorotributylamine (PFTBA) at the beginning of each analytical sequence. A minimum 5-point initial calibration consisting of selected target compounds was established to demonstrate the linear range of the analysis. Analyte concentrations in the standard solutions ranged from 0.01 to 10.0 ng/μL for PAH and 0.01 to 20.0 ng/μL for biomarkers. Quantification of target compounds was performed by the method of internal standards using average response factor (RF) determined in the initial calibration. Alkylated PAHs were quantified using the RF of the corresponding parent, triterpanes were quantified using the RF's for 17α(H),21β(H)-hopane, and steranes and triaromatic steroids were quantified using the RF of 5β(H)-cholane. Biomarker identifications were based upon comparison to selected authentic standards (*Chiron Laboratories*), elution patterns in the peer-reviewed literature, and mass spectral interpretation from full scan GC/MS analyses conducted in

our laboratory. Sample dry weights were determined separately and all concentrations are reported on a dry weight basis ($\mu g/kg_{dry}$).

All sediment sample/core locations and surrogate-corrected concentration data are publically available through NOAA Deepwater Horizon NRDA data portal, DIVER (Data Integration Visualization Exploration and Reporting), available at https://dwhdiver.orr.noaa.gov/. All concentrations used herein have been converted to non-surrogate-corrected values.

2.4 Degree of Weathering Quantification

The degree of weathering of the Macondo oil found was quantified based upon mass losses relative to the conservative internal marker within the oil, *viz.*, 17α(H),21β(H)-hopane (referred to hereafter as "hopane"), which has proven resistant to biodegradation (Prince et al. 1994). This approach was used to estimate the percent depletion of total PAHs ($TPAH_{50}$; see Table S-1 for definition) and individual PAH analytes using the following formula:

$$\%\text{Depletion of A} = [((A_0/H_0) - (A_s/H_s))/(A_0/H_0)] \times 100 \qquad \textit{Eq. (1)}$$

Where A_s and H_s is the concentrations of $TPAH_{50}$ or PAH analyte and hopane in the sediment sample ($\mu g/kg_{dry}$), respectively, and A_0 and H_0 are the concentrations of $TPAH_{50}$ or PAH analyte and hopane in the average, fresh Macondo source oil ($\mu g/g_{oil}$; from Stout et al., 2016). Although hopane can be degraded under some circumstances, if it (H_S) were degraded in a given sample, any % depletions calculated would be underestimated.

2.5 Forensic Method

Determining the presence or absence of Macondo oil in deep-sea sediments is not simply a matter of conventional chemical fingerprinting, e.g., comparing the chemical profile(s) of Macondo oil to the chemical profile(s) of a sediment sample to see if they "match." Even when such comparisons are appropriate (e.g., oily matrices), the degree to which samples "match" must carefully consider the effects of weathering, mixing, and analytical precision. Stout et al. (submitted) provides a detailed discussion of the weight-of-evidence forensic method by which Macondo oil was recognized in deep-sea

sediments – and distinguished from ambient (background) hydrocarbons and oil associated with natural oil seeps. An integral part of this method relied upon the knowledge (gained herein) of how the oil weathered within the deep-sea, thereby altering its chemical "fingerprint."

3. Results and Discussion

3.1 Conceptual Model for Seafloor Deposition of Macondo Oil

The presentation of the results are best prefaced by describing the conceptual model for deposition of Macondo oil on the seafloor that was revealed based upon the relationship between chemical fingerprints, concentrations, and the location of seafloor samples containing Macondo oil. This is practical since the character of Macondo oil, and thereby the basis for recognizing its presence in deep-sea sediments varied depending upon where the sample was collected. In this study, we focus on samples collected within about 8 km (5 miles) of the well, wherein significant changes due to weathering were revealed. The accompanying study (Stout et al., submitted) discusses results obtained in sediments collected further from the well.

Figure 2 illustrates the conceptual model depicting the general processes by which Macondo oil was deposited on the deep-seafloor. As will be shown below (Section 3.2), sediments collected within about ~1.6 km of the wellhead exhibit chemical characteristics that were readily recognized as Macondo oil or synthetic-based drilling mud (SBM) associated with direct fallout from the Macondo well. However, beyond ~1.6 km the surface sediments commonly contained increasingly weathered Macondo oil with distinctive chemical fingerprints. We have described this as a "*waxy-rich, severely weathered*" Macondo oil or "*oily floc*" (Fig. 2), which we describe in detail below (Section 3.3). This wax-rich, severely weathered oil could still be recognized as Macondo oil for multiple reasons, including (1) on average, the degree of weathering of the oil tends to increase with increasing distance from the well (Section 3.4), (2) the concentration of the oil in surface sediment intervals is highest closer to the wellhead and generally decreases away from the well, and (3) the concentration of severely weathered oil near the well is many times higher in the surface sediment intervals (0-1 and 1-3 cm) than in the deeper sediment intervals (Section 3.5).

These facts indicate that the wax-rich, severely weathered oil found on the seafloor surface away from the well (> 1.6 km) was formed by severe and rapid dissolution and biodegradation of the Macondo oil as it moved within the deep-sea, mostly within about 5 km of the well. We believe these weathering processes were accelerated within the (chemically and naturally) dispersed oil droplets, where the large surface area-to-mass ratio allowed for accelerated dissolution and biodegradation within the deep-sea plume (Payne and Driskell, 2015a,c; Prince et al. 2013; Driskell and Payne, in prep.).

Oil particles within the deep-sea plume eventually reached the seafloor (1) through scavenging and agglomeration with bacteria-rich marine snow formed in the deep-sea plume (supplemented by marine snow descending from the surface) and (2) by impingement of the plume on bathymetric features, including the continental slope (Fig. 2). In some instances the wax-rich, severely weathered Macondo oil settled atop sediments already containing variably-weathered crude oil from naturally-occurring seeps (see accompanying study; Stout et al., submitted). In the following sections, the chemical fingerprint characteristics of representative sediment samples and concentration trends exemplifying and justifying the conceptual model described above (Fig. 2) are presented.

In addition, our conceptual model acknowledges that sunken marine oil snow and *in situ* burn residues from the sea surface also contributed oil residues to the seafloor (Fig. 2). Other studies have shown that marine oil snow (Stout and German, in prep.) and *in situ* burn residues (Stout and Payne, 2016) were chemically distinguishable from the wax-rich, severely weathered Macondo oil residues derived from the deep-sea plume (described herein). In addition, the relative contribution of these surface oil deposition processes was secondary to the subsea oil deposited on the seafloor from the deep-sea plume.

3.2 Slightly Weathered Macondo Oil and Synthetic-Based Mud near the Wellhead

Forty-three (43) cores were collected within 1.6 km (1 mile) of the wellhead. All of these cores contained sediments impacted with Macondo oil and SBM, the latter exemplified by the varying amounts of C_{15} to C_{18} olefin clusters (Fig. 3B and C) that are characteristic features of SBM (Aeppli et al., 2013). In most cores the impact is restricted to the upper

3 cm of sediment. However, in multiple locations, Macondo oil and/or SBM was present in the 5-10 cm intervals (i.e., the deepest intervals studied) indicating significant thicknesses of oil and SBM (perhaps even > 10 cm) had been deposited on the seafloor in some areas within 1.6 km of the well.

The Macondo oil that was present in 20 of the 43 sediment cores within 1.6 km of the wellhead was only slightly weathered compared to the fresh oil (Fig. 3A) and could be easily recognized by the distribution of *n*-alkanes ranging from about *n*-C_{10} to *n*-C_{40} and a broad unresolved complex mixture (UCM) hump (Fig. 3B-C). Losses among the lower molecular weight fraction of the crude oil (<~*n*-C_{15}) and corresponding relative increase in the UCM are attributable to a combination of dissolution and incipient biodegradation (as evaporation is understood to have not affected oil in the deep-sea). Payne and Driskell (2015a) observed similar dissolution losses of *n*-alkanes (up to C_{12}) in particulate oil droplets isolated (filtered) from water samples collected at depth. Minor losses of lower molecular weight PAHs were also evident. This slightly weathered Macondo oil found in cores less than 1.6 km of the well, and often in association with SBM (e.g., Fig. 3B-C), is believed to represent oil that was quickly deposited on the seafloor due to direct fallout (perhaps aided by its association with SBM expelled during the initial blowout or during failed well plugging operations) after exiting the wellhead (Fig. 2).

3.3 Range in Weathering of Macondo Oil near the Wellhead

Sediments from the 23 remaining cores within 1.6 km of the wellhead contained oil that was much more weathered than the slightly weathered oil found in association with SBM (Fig. 3B-C). Recognition of the range in weathering among Macondo oil found in sediments near the wellhead was critical in developing the conceptual model (Fig. 2) that would ultimately allow recognition of Macondo oil's presence in sediments further away from the well. This range in weathering is demonstrated by the four surface sediment samples' chemical fingerprints shown in Figs. 4 to 6. These four samples are not unique as many other surface sediments near the wellhead exhibit comparable to those described here. The fact that surface sediments near the well contain variably weathered Macondo oil is testimony to the complex processes active within the subsea before and after oil reached the seafloor. These four samples, however, exemplify the progression in weathering that ultimately produced the wax-rich, severely weathered oil that was deposited on the seafloor further away from the well (Fig. 2).

Fig. 4 shows the progression in weathering of Macondo oil revealed by the GC/FID chromatograms of the TPH extracted from the representative sediments. There is a progressive loss of shorter-chain *n*-alkanes (Fig. 4A-C), ultimately producing a wax-rich oil containing an abundance of longer-chain *n*-alkanes spanning from ~n-C_{25} to n-C_{44} with a maximum ~ n-C_{33} (Fig. 4D). These longer-chain *n*-alkanes compounds are being preferentially *preserved* as the oil weathers, they are not being formed or absolutely enriched in the weathered oil (e.g., by some sort of wax-precipitation mechanism; see Fig. 7 described below). The preferential loss of *n*-alkanes below ~*n*-C_{30} is reasonably attributable to intense biodegradation, which can preserve the longer chain *n*-alkanes as shorter chain *n*-alkanes are preferentially degraded (Prince, 2002; Prince et al., 2013). However, under the circumstances of this particular spill, some loss of shorter-chain *n*-alkanes might also be attributed to dissolution enhanced by the use of dispersant near the wellhead (Fu et al., 2014) despite these compounds' limited (but extant) solubility. Payne and Driskell (2015a) observed similar losses of *n*-alkanes (up to C_{12}) in particulate (filtered) oil droplets sampled from the water column at depth indicating the preferential loss of shorter chain *n*-alkanes occurred, or at least was initiated, while the oil was within the water column.

Accompanying the loss of *n*-alkanes was the progressive loss of isoprenoids (e.g., pristane and phytane) and the bulk of unresolved and resolved compounds within the C_{10} to C_{25} range, commonly referred to as diesel range organics (DRO; Fig. 4). This loss in DRO can be seen in the reduction in the size of the UCM in the DRO range – and corresponding retention/enrichment of the compounds within the residual range oil (RRO; C_{25}+; Fig. 4). The progressive loss in DRO compounds is also reasonably attributed to the combined effects of dissolution and biodegradation of the Macondo oil, which would be predicted to remove these lower molecular weight DRO compounds in preference to the higher molecular weight RRO compounds. Prince et al. (2013) observed a comparable reduction in DRO range hydrocarbons due to biodegradation in laboratory experiments of chemically-dispersed North Slope crude oil.

The preferential loss of DRO-range compounds in the TPH (Fig. 4) is clearly evident upon inspection of these samples' hopane-normalized PAH histograms, which show a progressive loss of increasingly heavier PAHs during weathering of the Macondo oil near

the well (Fig. 5). Each homologue group becomes increasingly skewed toward the more highly alkylated derivatives, as is typically observed and attributed to biodegradation in field and laboratory weathering studies (Bayona et al., 1986; Elmendorf et al., 1994; Wang et al., 1998; 2001; Diez et al., 2005; Prince et al., 2013). Evidence that dissolution contributed to the losses was reported by Payne and Driskell (2015a) who observed filtered water samples from the deep-sea enriched in dissolved decalins and lower molecular weight PAHs, and PAHs with lower degrees of alkylation.

The progression in weathering ultimately led to the loss of all of the decalins and benzothiophenes, and nearly all lower molecular weight PAHs (naphthalenes, fluorenes, phenanthrenes, and dibenzothiophenes; e.g. Fig. 5D). The remaining higher molecular weight PAHs (fluoranthenes/pyrenes, naphthobenzothiophenes, benz[a]anthracenes/ chrysenes) in the wax-rich, severely weathered Macondo oil were also significantly reduced from the fresh Macondo oil despite these PAHs' low aqueous solubilities. Severe weathering of Macondo oil in the deep-sea ultimately produced an oil residue dominated by C_3- and C_4-benz[a]anthracenes/ chrysenes (BC3 and BC4; Fig. 5D). This pattern is not unexpected as both aqueous solubility and susceptibility to biodegradation decreases with increasing molecular weight and degree of alkylation; however, the extent to which dissolution and/or biodegradation affected the Macondo oil in a relatively short period of time is remarkable – and (as noted above) we attribute this to the finely dispersed nature of the oil within the deep-sea plume, which accelerated both processes.

The petroleum biomarkers in the Macondo oil in sediments near the well also exhibited some progressive changes upon weathering, as exemplified in Fig. 6. These changes were important to recognize since biomarkers are sometimes considered *recalcitrant* to weathering, not simply *resistant*. Biomarker degradation under different environmental conditions is extremely complex and can be difficult to predict *a priori*. Therefore, only after recognizing/documenting the progressive changes in the Macondo oil biomarkers (among samples found close to the wellhead) could the altered biomarker fingerprint of the wax-rich, severely weathered Macondo oil found further from the well be confidently attributed to Macondo oil.

Inspection of Fig. 6 shows that the tri- and pentacyclic terpane biomarkers remained fairly consistent during weathering of the Macondo oil in the deep-sea, although a loss of C_{28} and C_{29} tricyclic terpanes (T7 to T10) and C_{34} and C_{35} 17α(H),21β(H)-homohopane homologues (T32-T35) was often evident (Fig. 6E). The loss of these same terpanes with extended alkyl side chains was observed in laboratory biodegradation studies of chemically dispersed oil (Prince et al., 2013) indicating selective biodegradation – most likely affecting those terpanes with extended alkyl side chains – appears to also have affected the Macondo oil in the deep-sea. Notably, the loss of these biomarkers was previously observed in non-dispersed spilled oils but over long time periods (Munoz et al., 1997; Wang et al., 2001), indicating the rate of extended terpane biodegradation was accelerated by the dispersed nature of the Macondo oil that remained in the deep-sea.

Another observation regarding terpanes is that at lower oil concentrations the contribution (interference) of naturally-occurring triterpenoids derived from recent organic matter (e.g., algal or microbial biomass) was greater. These compounds are often recognized to occur as "modern" background throughout the deep-sea sediments (Simoneit, 1986; Hood et al. 2002; Dembicki, 2010). These compounds can co-elute with petroleum-derived triterpanes and artificially increase the relative abundance/concentrations of some targeted triterpanes (T20 and T26). A commonly prominent interfering terpane co-elutes with moretane (T20; Fig. 6D-E) and is likely 17β(H),21β(H)-30-norhopane, a naturally-occurring triterpane that can be prominent in recent marine sediments (Kennicutt and Comet, 1992).

Steranes exhibited multiple changes due to weathering. The most notable of which was a marked reduction in the relative abundances of 13β(H),17α(H)-diacholestane epimers (S4 and S5) and 14β(H),17β(H)-cholestane epimers (S14 and S15; Fig. 6). Some reduction was also evident in the co-eluting epimers of 14α(H),17β(H)-cholestane and 13β(H),17α(H)-diaethylcholestane (S12/S13 and S17/S18; Fig. 6). The preferential loss of 13β(H),17α(H)-diacholestanes and 14β(H),17β(H)-cholestanes has been observed previously in spilled oil and attributed to biodegradation, although over much longer time scales (Wang et al. 2001; Prince et al., 2002) and *in vitro* (Diez et al. 2005). As was the case for other hydrocarbons (see above), the rapid biodegradation of these $\beta\alpha$ dia- and $\beta\beta$ regular C_{27} steranes in the Macondo oil over a short period of time is, as with other

weathering changes, attributed to accelerated biodegradation within the finely dispersed oil droplets in the deep-sea plume. Notably, a comparable loss of 13β(H),17α(H)-diacholestanes and 14β(H),17β(H)-cholestanes was also reported by White et al. (2012) in floc on deep-sea coral samples collected from northwest Biloxi Dome in later 2010. These researchers hypothesized this was due to biodegradation in the Macondo oil, which is confirmed herein to also have affected Macondo oil found much closer to the Macondo wellhead (Fig. 6). Finally, the wax-rich, severely weathered oil found in some sediments near the well showed some reduction in the amount of triaromatic steroids (TAS) compared to fresh Macondo oil. This loss is described further in the following section.

3.4 Weathering among Macondo Oil in Sediments further from the Wellhead

Eighty-eight (88) cores were collected between 1.6 and 4.8 km (1-3 miles) and 95 cores were collected between 4.8 and 8.0 km (3-5 miles) of the well. The latter included 47 cores collected along the margins of Mitchell, Gloria, and Biloxi Domes (Fig. 1), which owing to the potential influence of seep oils on sediments in these areas, were excluded from the evaluation of Macondo oil weathering discussed herein. These seep area cores were evaluated in the accompanying study (Stout et al., submitted).

Forty-six cores collected between 1.6 and 8.0 km of the well contained wax-rich, severely weathered Macondo oil at their surface (0-1 cm) that was largely consistent with what was observed nearer the wellhead (resembling Figs. 4D, 5D, and 6E). However, as described below, on average, there was some additional progression in the weathering of the oil at increasing distances from the well. The remaining cores 1.6 to 8 km from the well contained only “background” (ambient) hydrocarbons, the character of which is described in Stout et al. (submitted), or only traces of Macondo oil mixed with background hydrocarbons. This spatial heterogeneity in the amount of Macondo oil residues deposited – sometimes among co-located cores collected within a few meters of one another – indicates that the deposition/accumulation of wax-rich, severely weathered Macondo oil was non-uniform, which would seem consistent with particle deposition of the oil (Fig. 2).

Twenty-six (26) cores between 1.6 and 4.8 km and 20 cores between 4.8 and 8.0 km contained elevated concentrations of wax-rich, severely weathered Macondo oil. An

inventory of these cores is given in Table S-2. Because it was our intention to characterize the weathering of Macondo oil, those cores containing lower concentrations of Macondo oil mixed with background hydrocarbons were excluded because their hydrocarbon fingerprints were affected by mixing of Macondo oil and background, and not by Macondo oil weathering. The knowledge gained from understanding the progression in weathering observed closer to the well (Section 3.3; Figs. 4-6) confirmed that the wax-rich, severely weathered oil found in surface sediments between 1.6 to 8.0 km from the well was also derived from Macondo oil. Establishing this, in turn, aided in developing the conceptual model described above (Section 3.1; Fig. 2). The results also revealed that the overall weathering of the wax-rich, severely weathered oil generally increased with increasing distance from the well. This observation also contributed to the conceptual model, *viz.*, weathering (dissolution and biodegradation) appears to have occurred mostly during the Macondo oil's lateral advective transport within the deep-sea plume (Fig. 2), and not mostly after deposition on the seafloor.

The degree of weathering of the Macondo oil naturally varied at any given distance from the well, however, the progressive increase in weathering of the oil as it moved away from the well is revealed by the *average* chemical fingerprints of the wax-rich, severely weathered oil found in surface sediments collected at increasing distance from the well. We present data for cores collected from three distance intervals, viz., less than 1.6 km from the well, between 1.6 to 4.8 km, and between 4.8 to 8.0 km, as each of these three intervals contained a sufficient and comparable number of impacted cores (n=23, 26, and 20, respectively; Table S-2). Average concentrations for *n*-alkanes, PAHs, and biomarkers for sediments 0 to 1.6, 1.6 to 4.8, and 4.8 to 8.0 km that contained the wax-rich, severely weathered oil are given in Tables S-3, S-4, and S-5, respectively. Concentrations of these compounds in fresh Macondo oil (Stout et al., 2016) are given for comparison. Figs. 7, 8, and 10 show the hopane-normalized average distributions of *n*-alkanes, PAHs, and biomarkers in these three sample groups, respectively. Figure 9 provides the average percent depletion results (per *Eq. 1*) for PAHs in each group. These figures are described in the following paragraphs.

Figure 7 shows that most *n*-alkanes are indeed markedly depleted in the wax-rich, severely weathered Macondo oil found in sediments with only the longer-chain n-alkanes (>*n*-C_{25}) being preserved. It is clear that these longer-chain *n*-alkanes are not *enriched*

relative to fresh Macondo oil, but are only *preserved* owing to their lower susceptibility to both dissolution and biodegradation. Notably, closer to the well there is some evidence of SBM's presence as exhibited by the relative abundances of *n*-C_{16} and *n*-C_{18} (Fig. 7A-B), which is caused by co-elution of SBM-derived olefins with these *n*-alkanes in GC/FID).

Figure 8 shows the changes in the hopane-normalized abundance and distributions of PAHs in the wax-rich, severely weathered Macondo oil found in sediments at increasing distances from the well. The average absolute concentrations observed within these sediments are given in Table S-4. Within 1.6 km of the well the PAHs exhibit marked losses relative to fresh Macondo oil although some decalins, benzothiophenes, naphthalenes and other lower molecular weight PAHs are still clearly present (Fig. 8A). Between 1.6 to 4.8 km and 4.8 to 8.0 km from the well, however, decalins and low molecular weight PAHs become increasingly reduced (Fig. 8B-C). Higher molecular weight PAHs also become progressively reduced up to 4.8 km from the well (Fig. 8A-B), but then do not show much additional reduction beyond this distance (Fig. 8C). Decalins, benzothiophenes, and naphthalenes, however, are (on average) virtually absent in the wax-rich, severely weathered Macondo oil beyond 4.8 km from the wellhead (Fig. 8C; Table S-4).

Figure 9 shows the calculated average percent depletion of individual and total PAH ($TPAH_{50}$) within the wax-rich, severely weathered Macondo oil found in surface sediments within 8 km of the well (per *Eq. 1*). $TPAH_{50}$ depletions within 1.6 km of the well averaged 86 ± 8% (Fig. 9A), indicating most PAHs present in the oil that remained in the deep-sea did not accumulate on the seafloor. We attribute these depletions to the combined effects of dissolution and biodegradation, the latter of which may have converted the targeted PAHs into non-targeted (polar) derivatives not measured in our study. The percent depletions were greatest among lower molecular weight PAHs and systematically decreased with increasing degree of alkylation within each homologue group (Fig. 9A). The decreased depletions with increased alkylation is consistent with what would be expected for both dissolution and biodegradation, therefore it is not possible to distinguish which of these processes, if either, is dominantly responsible for their losses from the oil.

The average percent depletion of PAHs in Macondo oil found in surface sediments between 1.6 and 4.8 km of the well increased compared to oil found closer to the well. In these sediments between 87 and 100% depletion of decalin, benzothiophene, naphthalene, fluorene, phenanthrene, and dibenzothiophene homologues and increased percent depletions among higher molecular weight PAHs were observed (Fig. 9B). Average percent depletion of total PAH ($TPAH_{50}$) increased to 94 ± 3% (Fig. 9B). The Macondo oil in sediments collected between 4.8 and 8.0 km from the well, however, demonstrate only minor increase in the average percent depletion of $TPAH_{50}$ to 95 ± 1% (Fig. 9C).

The overall increase in PAH weathering (Fig. 8) and depletion (Fig. 9) *versus* distance from the well indicates that dramatic losses occurred in the oil deposited within about 5 km of the well (Fig. 9A-B), but that no significant additional loss of PAHs from the wax-rich, severely weathered Macondo oil occurred beyond about 5 km from the well. As per the conceptual model described above (Fig. 2), we interpret this trend as evidence that the loss of PAHs from the dispersed oil in the deep-sea overwhelmingly occurred via dissolution and biodegradation during its early residence and initial transport within the deep-sea water column/plume relatively close to the well (< 5 km; and not only after deposition in the sediment). If the weathering had occurred predominantly after the oil had been deposited on the seafloor (rather than within the plume) we would expect no such trend with distance as we observe (Figs. 7-9). We contend the combined processes of dissolution and biodegradation were so rampant within the plume less than ~5 km of the well that the finely dispersed oil droplets “surviving” to be laterally transported further from the well (some being subsequently deposited in sediments) were only minimally further weathered. As such, beyond about 5 km from the well there is a remarkable consistency to the character of the PAHs within the wax-rich, severely weathered Macondo oil deposited in sediments (e.g., Fig. 8C).

Figure 10 shows the average hopane-normalized abundance of biomarkers present in the wax-rich, severely weathered Macondo oil deposited on the seafloor at increasing distance from the well. The average absolute concentrations observed within these sediments are given in Table S-5. The biomarkers were much less affected than the *n*-alkanes or PAHs (described above) but nonetheless exhibit some progressive changes with increasing distance from the well. As was evident in Fig. 6E, among the terpanes

there were reductions in the relative abundances of C_{28} and C_{29} tricyclic terpanes (T7 to T10) and C_{34} and C_{35} homohopanes with increasing distance from the well (T31 to T35; Fig. 10). As with the PAHs, the loss of these terpanes occurred predominantly within 5 km of the well (Fig. 10A-B). The preferential loss of these same two groups of terpanes, i.e., those with extended alkyl side chains, was observed in laboratory biodegradation studies on dispersed oil (Prince et al., 2013), supporting our contention that biodegradation of the dispersed Macondo oil droplets within the deep-sea plume within 5 km of the well altered these distributions. As noted above, some triterpane interferences are also evident in sediments due to pre-existing, naturally-occurring triterpenoids in deep-sea sediments (e.g., T20 and T26 in particular; Fig. 10).

Among the steranes there was a marked depletion of the 13β(H),17α(H)-diacholestanes (S4 and S5), 14β(H),17β(H)-cholestanes (S14 and S15), and co-eluting 14α(H),17β(H)-cholestanes and 13β(H),17α(H)-diaethylcholestanes (S12/S13 and S17/S18) observed in the wax-rich, severely weathered oil deposited on the seafloor less than 1.6 km from the well (Fig. 10A). The loss increased for the oil found in sediments between 1.6 and 4.8 km from the well (Fig. 10B) and then remained largely stable in sediments between 4.8 and 8.0 km from the well (Fig. 10C). Thus, as with the PAHs described above, most of the loss of these particular steranes occurred within ~5 km of the well. Unfortunately, Prince et al. (2013) did not report on the effects of biodegradation on steranes in chemically dispersed oil, however, biodegradation of 13β(H),17α(H)-diacholestanes and 14β(H),17β(H)-cholestanes was previously observed in non-dispersed spilled oil although over much longer time scales (Wang et al. 2001; Prince et al., 2002). As noted above, White et al. (2012) observed that oily floc recovered from deep-sea corals from northwest Biloxi Dome (~13 km from the wellhead; Fig. 1) in later 2010 also exhibited depleted13β(H),17α(H)-diacholestanes and 14β(H),17β(H)-cholestanes. Our results indicate these steranes were likely biodegraded from dispersed oil droplets while in the deep-sea plume within about 5 km of the well before being laterally transported and deposited on the corals further away.

Finally, the relative abundances of all four targeted C_{26} to C_{28} triaromatic steroids (TAS) in the wax-rich, severely weathered Macondo oil found less than 1.6 km from the well were slightly reduced compared to the fresh oil (Fig. 10A). TAS in oiled sediments between 1.6 and 4.8 km from the well were further reduced (Fig. 10B) but then largely

remained stable between 4.8 and 8.0 km from the well (Fig. 10C). Thus, like the PAHs, the TAS within the wax-rich, severely weathered Macondo oil deposited beyond about 5 km from the well are unlikely to have been much further weathered (Fig. 10C). C_{26} to C_{28} TAS congeners were markedly and equitably reduced in floating and stranded Macondo and attributed to their comparable susceptibilities to photo-oxidation (Aeppli et al. 2014; Stout et al., 2016), which was confirmed in laboratory irradiation studies (Radović et al., 2014). Photo-oxidation, however, could not have affected the TAS in Macondo oil that had remained in the deep-sea, indicating their reduction must be attributed to dissolution or biodegradation. C_{26} to C_{28} TAS are considered largely recalcitrant to biodegradation (Douglas et al., 2012) suggesting dissolution may be more likely responsible for their reduction (Fig. 10). This conclusion is supported by the fact that the average percent depletions (relative to hopane; Eq. 1) of the C_{26} and C_{27} TAS congeners exceeded those of the C_{28} TAS congeners in sediments regardless of the distance from the well (Table S-6). Correspondingly, the aqueous solubilities and octanol-water partitioning coefficients for the C_{26} and C_{27} TAS congeners also exceed those of the C_{28} TAS congeners (Table S-6). Thus, as was the case with other higher molecular weight aromatic compounds often thought to be practically insoluble (Figs. 8-9), we contend these aromatic biomarkers were also dissolved from the dispersed oil droplets transported within the deep-sea plume, mostly within 5 km of the well. Notably, Payne and Driskell (2015a) also noted dissolution-mediated loss of TAS congeners in particulate oil droplets isolated by filtration of water samples collected at depth.

3.5 Concentration Trends

In addition to the chemical fingerprint trends, concentration trends within each core were also considered in evaluating the impact of Macondo oil on sediments near the well. Figure 11 shows the $TPAH_{50}$ concentration profiles in those cores containing the wax-rich, severely weathered Macondo oil found 0 to 1.6, 1.6 to 4.8, and 4.8 to 8.0 km from the well (Table S-2). These same populations of cores were used to develop the average concentrations and distributions of PAHs in Macondo oily floc (Table S-4; Fig. 8.). Those surface sediments containing high concentrations of slightly weathered Macondo oil deposited within 1.6 km of the well (Section 3.2) or containing only a trace of Macondo oil residue mixed with background are excluded, therefore the average $TPAH_{50}$ concentrations indicated are best interpreted in a relative sense.

The concentrations of PAHs are highest in surface sediments nearest the well (Fig. 11A) and decrease with increasing distance from the well (Figs. 11B-C). Although highly varying, the average $TPAH_{50}$ concentrations within 1.6 km of the well (31,400 ± 52,000 μg/kg) were markedly higher than found 1.6 to 4.8 km (2900 ± 1400 μg/kg) or 4.8 to 8.0 km (2500 ± 1300 μg/kg) from the well (Table S-4). All of the cores, however, exhibit higher concentrations of PAH at the surface (0-1 cm) than below the surface, which is consistent with its geologically-recent deposition. Only a few cores less than 1.6 km from the well appear to have elevated PAH concentrations below 0-1 cm, indicating thicker accumulations. Most other cores and those beyond 1.6 km appear to contain only ambient (background) concentrations of total PAH in the deepest (5-10 cm) core intervals studied, averaging 180 ± 100 (1.6 to 4.8 km) and 190 ± 80 μg/kg (4.8 to 8.0 km) from the well (Fig. 11B-C). Even ignoring the chemical fingerprinting trends described above, the observed PAH concentration (lateral and vertical) trends indicate the oil in these surface sediments could only be reasonably attributed to the DWH oil spill and not to any pervasive background or geologically-long-lived seeps. Both concentration trends (Fig. 11) are consistent with the conceptual model in which Macondo oil residues were deposited at the surface only and tended to decrease with increasing distance from the well (Fig. 2).

4. Conclusions

The study of deep-sea sediments from cores collected in 2010/2011 within 8 km of the Macondo well following the *Deepwater Horizon* oil spill has affirmed a conceptual model in which Macondo oil residues (not just dissolved hydrocarbons and gases) that remained within the deep-sea was not only deposited on the seafloor around the well but also was laterally distributed by the deep-sea plume(s) and subsequently deposited on the seafloor away from the well. Specifically, 20 of the 43 cores collected within 1.6 km of the wellhead contained a slightly weathered Macondo oil mixed with varying amounts of synthetic-based drilling mud (SBM) mostly within the top 3 cm, but up to 10 cm deep (at least) in some locations. This slightly weathered oil experienced some loss of *n*-alkanes and other hydrocarbons below about *n*-C_{15} but otherwise was consistent with the spilled oil. The association of this slightly weathered oil with SBM suggests (enhanced and) direct fallout of oil (and SBM) was prevalent close to, i.e., mostly less than 1.6 km from, the well.

Surface (0-1 or 0-2 cm) sediments and some sub-surface sediments (1-3 or 2-4 cm) from the remaining 23 cores collected within 1.6 km of the well contained more highly-weathered Macondo oil that experienced varying weathering effects in excess of the slightly weathered oil observed in the other cores. These effects included excessive dissolution and/or biodegradation that is attributed to weathering that acted upon physically and/or chemically dispersed oil droplets formed as the oil was expelled and became entrained within the deep-sea plume that formed ~200 to 500 m above the wellhead. Owing to the small droplet size (i.e., large surface area-to-volume) of the dispersed droplets, dissolution and biodegradation was rapid and extensive, imparting significant changes to the composition of the oil that ultimately produced a wax-rich, severely weathered oil.

The effects of this weathering increased with increasing distance from the Macondo well as evidenced by the average compositions of the wax-rich, severely weathered oil in surface sediments in 26 cores collected 1.6 to 4.8 km and 20 cores collected 4.8 to 8.0 km from the well. The greatest changes were evident in the oil found in surface sediments within approximately 5 km from the well with only marginal increased weathering observed in oiled sediments between ~5 and 8 km. This indicates that most of the dissolution and biodegradation that affected the dispersed oil droplets occurred rapidly during their lateral advective transport within the deep sea plume (not after deposition on the seafloor) within 5 km of the well. The wax-rich, severely weathered oil droplets entrained in the deep-sea plume transported beyond 5 km from the well were only slowly and minimally weathered further.

Concentration of Macondo oil in sediments within 8 km of the well, as reflected herein by total PAH concentrations in the impacted cores (1) were markedly higher in surface sediments (0-1 cm) than in deeper sediments and (2) tended to decrease within increasing distance from the well. These vertical and lateral concentration trends further support the conceptual model by which most Macondo oil was deposited on the seafloor after lateral advective transport within the deep-sea plume.

The severe weathering observed included the progressive loss of (1) shorter-chain *n*-alkanes and prominent acyclic isoprenoids (e.g., pristane and phytane) and preferential

preservation of longer-chain *n*-alkanes spanning from ~*n*-C_{25} to n-C_{44} with a maximum ~*n*-C_{33}, (2) unresolved compounds within the C_{10} to C_{25} range, commonly referred to as diesel range organics (DRO) that strongly shifted the UCM profile observed via GC/FID toward the residual range organics (C_{25}+; RRO), (3) increasingly heavier PAHs with each homologue group becoming increasingly skewed toward the more highly alkylated derivatives. Relative to hopane this ultimately led to the 100% depletion of decalins and benzothiophenes, nearly 100% depletion of C_0- to C_4- naphthalenes, fluorenes, phenanthrenes, and dibenzothiophenes, and varying depletions among C_0- to C_4- fluoranthenes/pyrenes, naphthobenzothiophenes, and benz[a]anthracenes/chrysenes, which ultimately produced a Macondo oil residue dominated by C_3- and C_4- benz[a]anthracenes/chrysenes. And, finally, the severe weathering observed included the progressive loss of (4) selected biomarkers including C_{28}- and C_{29}- tricyclic terpanes, C_{34}- and C_{35}- 17α(H),21β(H)-homohopane homologues, C_{27}- 13β(H),17α(H)-diasteranes, C_{27}- 14β(H),17β(H)-steranes, co-eluting C_{27}- 14α(H),17β(H)-steranes and C_{29}- 13β(H),17α(H)-diasteranes, and C_{26} to C_{28} triaromatic steroids (TAS). Preferential biodegradation of the aforementioned terpanes, hopanes, dia- and regular steranes is consistent with other long-term or laboratory weathering studies whereas the loss of TAS, which we attribute to dissolution of these aromatic compounds (as photo-oxidation in the deep-sea is unreasonable), was heretofore unrecognized.

The weathering changes described herein imparted a distinct chemical fingerprint for the wax-rich, severely weathered Macondo oil found at the surface of all impacted cores between about 5 and 8 km from the well. Recognizing the severity and effects of weathering on the Macondo oil within the deep-sea will allow it to be recognized in sediments further from the well despite low(er) concentrations and also to be distinguished from pervasive background hydrocarbons and seep oils (see accompanying study; Stout et al., submitted).

Acknowledgments

The authors wish to thank the efforts of numerous Trustee and BP field teams that cooperatively planned and collected the deep-sea samples used in this analysis, an effort unprecedented in oil spill investigations. The efforts of Christopher Lewis (Industrial Economics, Corp.) and Robert Ricker (NOAA) in organizing the sample collection efforts are specifically acknowledged. The authors also wish to thank Greg

Baker (NOAA), Nancy Rothman (New Horizons), William B. Driskell (Driskell Consultants), Ann Jones (Industrial Economics, Corp.) for coordinating the large analytical program. The efforts of numerous NewFields staff who aided in the management of the chemical analyses (Wendy Wong and Eric Litman), database (George Desreuisseau and Gang Hu), and GIS (Bo Liu) are also acknowledged.

Disclosure

This study was conducted within the *Deepwater Horizon* NRDA investigation, which was cooperatively conducted by NOAA, other Federal and State Trustees, and BP. The scientific results and conclusion of this publication, as well as any views or opinions expressed herein, are those of the authors and do not necessarily represent the view of NOAA or any other natural resource Trustee for the BP/Deepwater Horizon NRDA. The authors declare no competing financial interest in the publication of this study. Funding for the study was provided by NOAA as part of the NRDA process.

References

Aeppli, C., Carmichael, C.A., Nelson, R.K., Lemkau, K.L., Graham, W.M., Redmond, M.C., Valentine, D.L., Reddy, C.M., 2012. Oil Weathering after the Deepwater Horizon Disaster Led to the Formation of Oxygenated Residues. Environ. Sci. Technol. 46(16): 8799-8807.

Aeppli, C., Reddy, C.M., Nelson, R.K., Kellermann, M.Y., Valentine, D.L., 2013. Recurrent oil sheens at the Deepwater Horizon disaster site fingerprinted with synthetic hydrocarbon drililng fluids. Environ. Sci. Technol. 47(15): 8211-8219.

Aeppli, C., Nelson, R.K., Radović, J.R., Carmichael, C.A., Valentine, D.L., Reddy, C.M., 2014. Recalcitrance and degradation of petroleum biomarkers upon abiotic and biotic natural. weathering of Deepwater Horizon oil. Environ. Sci. Technol. 48: 6726-6734.

Atlas, R. M. and Hazen, T.C., 2011. Oil biodegradation and bioremediation: A tale of the two worst spills in U.S. history. Environ. Sci. Technol. 45: 6709-6715.

Baelum, J., Borglin, S., Chakraborty, R., Fortney, J.L., Lamendella, R., Mason, O.U., Auer, M., Zemla, M., Bill, M., Conrad, M.E., Malfatti, S.A., Tringe, S.G., Holman, H.Y., Hazen, T.C., Jansson, J.K., 2012. Deep-sea bacteria enrich by oil and dispersant from the Deepwater Horizon spill. Environ. Microbiol. 14(9): 2405-2416.

Bayona, J.M., J. Albaiges, A.M. Solanas, R. Ares, P. Garrigues, M. Ewald, 1986. Selective aerobic biodegradation of methyl-substituted polycyclic aromatic hydrocarbons in petroleum by pure microbial cultures. Int. J. Environ. Anal. Chem., 23: 289-303.

Boehm, P.D., K.J. Murray, L.L. Cook, 2016. Distribution and attenuation of polycyclic aromatic hydrocarbons in Gulf of Mexico seawater from the *Deepwater Horizon* oil accident, Environ. Sci. Technol. 50 (2): 584-592.

Camilli, R., C. M. Reddy, D. R. Yoerger, B. A. S. Van Mooy, M. V. Jakuba, J. C. Kinsey, C. P. McIntyre, S. P. Sylva and J. V. Maloney, 2010. Tracking Hydrocarbon Plume Transport and Biodegradation at Deepwater Horizon. Science 330: 201-204.

Carmichael, C.A., Arey, J.S., Graham, W.M., Linn, L.J., Lemkau, K.L., Nelson, R.K., Reddy, C.M. 2012. Floating oil-covered debris from Deepwater Horizon: Indentification and application. Environ. Res. Lett. 7, 015301, 6 p.

Daling, P.S., Leirvik, F., Almas, I.K.,. Brandvik, P.J., Hansen, B.H., Lewis, A., Reed, M. 2014. Surface weathering and dispersibility of MC252 crude oil. Mar. Pollut. Bull. 87: 300-310.

Dembicki, H., 2010. Recognizing and compensating for interference from sediment's background organic matter and biodegradation during interpretation of biomarker data from seafloor hydrocarbon seeps: An example from the Marco Polo area seeps, Gulf of Mexico, USA. Mar. Petrol. Geol. 27: 1936-1951.

Diercks, R.C., Asper, V.L., Joung, D., Zhou, Z., Guo, L., Shiller, A.M., Joye, S.B., Teske, A.P., Guinasso, N., Wade, T.L., Lohrenz, S.E., 2010. Characterization of subsurface polycyclic aromatic hydrocarbons at the Deepwater Horizon site. Geophys. Res. Lett. 37: L20602.

Díez, S., Sabate, J., Vinas, M., Bayona, J. M., Solanas, A. M., Albaiges, J., 2005. The Prestige oil spill. I. Biodegradation of a heavy fuel oil under simulated conditions. Environ. Toxicol. Chem. 24: 2203-2217.

Douglas, G.D., J.H. Hardenstine, B. Liu, A.D. Uhler, 2012. Laboratory and field verification of a method to estimate the extent of petroleum biodegradation in soil. Environ. Sci. Technol. 46: 8279-8287.

Douglas, G.S., Emsbo-Mattingly, S.D., Stout, S.A., Uhler, A.D., McCarthy, K.J., 2015. Chemical fingerprinting methods. In: Introduction to Environmental Forensics, 3rd Ed., (B.L. Murphy and R.D. Morrison, Eds.), Acad. Press, P. 201-309.

Driskell, W.B., Payne, J.R., in preparation. Dispersant-accelerated PAH dissolution in the *Deepwater Horizo*n Plume.

Elmendorf, D.L., Haith, C.E., Douglas, G.S., Prince, R.C.,1994. Relative rates of biodegradation of substituted polycyclic aromatic hydrocarbons. In: Bioremediation of Chlorinated and Polycyclic Aromatic Hydrocarbon Compounds, R.E. Hinchee et al. (Eds.), Boca Raton, FL: Lewis Publishers, pp. 188-202.

Faksness, L.G., Altin, D., Nordtug, T., Daling, P.S., Hansen, B.H. 2015. Chemical comparison and acute toxicity of water accommodated fraction (WAF) of source and field collected Macondo oils from the Deepwater Horizon oil spill. Mar. Pollut. Bull. 91: 222-229.

Fu, J., Gong, Y., Zhao, X., O'Reilly, S.E., Zhao, D., 2014. Effects of oil and dispersant on formation of marine oil snow and transport of oil hydrocarbons. Environ. Sci. Technol., 48(24): 14392-9.

Hall, G.J., Frysinger, G.S., Aeppli, C., Carmichael, C.A., Gros, J., Lemkau, K.L., Nelson, R.K., Reddy, C.M. 2013. Oxygenated weathering products of Deepwater Horizon oil come from surprising precursors. Mar. Poll. Bull. 75: 140-149.

Hazen, T.C., Dubinsky, E.A., DeSantis, T.Z., Andersen, G.L., Piceno, Y.M. et al., 2010. Deep-sea oil plume enriches indigenous oil-degrading bacteria. Science 330: 204-208.

Hood, K.C., Wenger, L.M., Gross, O.P., Harrison, S.C., 2002. Hydrocarbon systems analysis of the northern Gulf of Mexico: Delineation of hydrocarbon migration pathways using seeps and seismic imaging. In: Surface Exploration Case Histories, D. Schumacher and L.A. LeSchack, Eds., AAPB Studies in Geology, No. 48, and SEG Geophysical Ref. Series, No. 11: 25-40.

Kennicutt, M. C. and P. A. Comet, 1992. Resolution of sediment hydrocarbons sources: Multiparameter approach. Organic Matter: Productivity, Accumulation, and Preservation in Recent and Ancient Sediments. J. K. Whelan and J. W. Farrington. New York, Columbia Univ. Press: 309-338.

Kessler, J.D., Valentine, D.L., Redmond, M.C., Du, M., Chan, E.W., Mendes, S.D., Quiroz, E.W., Villanueva, C.J., Shusta, S.S., Werra, L.M., Yvon-Lewis, S.A., Weber, T.C. 2011. A persistent oxygen anomoly reveals the fate of spilled methane in the deep Gulf of Mexico. Science, 331: 312-315.

Kiruri, L.W., Dellinger, B. Lomnicki, S., 2013. Tar balls from Deep Water Horizon oil spill: environmentally persistent free radicals (EPFR) formation during crude weathering. Environ. Sci. Technol. 47(9): 4220-4226.

Lewan, M.D., Warden, A., Dias, R.F., Lowry, Z.K., Hannah, T.L., Lillis, P.G., Kokaly, R.F., Hoefen, T.M., Swayze, G.A., Mills, C.T., Harris, S.H., Plumlee, G.S., 2014. Asphaltene content and composition as a measure of Deepwater Horizon oil spill losses within the first 80 days. Org. Geochem. 75: 54-60.

Lindo-Atichati, D., Paris, C.B., LeHenaff, M., Schedler, M., Valladares Juarez, A.G., Muller, R., 2014. Simulating the effects of droplet size, high pressure biodegradation, and variable flow rate on the subsea evolution of deep plumes from the Macondo blowout. Deep Sea Research II, doi./10.1016/j.dsr2.2014.01.001.

Liu, Z.F., Liu, J.Q., Zhu, Q.Z., Wu, W., 2012. The weathering of oil after the Deepwater Horizon oil spill: Insights form the chemical composition of the oil from the sea surface, salt marshes and sediments. Environ. Res. Lett. 7(doi:10.1088/1748-9326/7/3/035302): 14 pp.

McKenna, A.M., Nelson, R.K., Reddy, C.M., Savory, J.J., Kaiser, N.K., Fitzsimmons, J.E., Marshall, A.G., Rodgers, R.P., 2013. Expansion of the analytical window for oil spill characterization by ultrahigh resolution mass spectrometry: Beyond gas chromatography. Environ. Sci. Technol. 47: 7530-7539.

Munoz, D., Guiliano, M., Doumenq, P., Jacquot, F., Scherrer, P., Mille, G., 1995. Long-term evolution of petroleum biomarkers in mangrove soil (Guadeloupe). Mar. Pollut. Bull. 34(11): 868-874.

OSAT-1, 2010. Summary report for sub-sea and sub-surface oil and dispersant detection: Sampling and monitoring. Operational Science Advisory Team, Dec. 17, 2010.

Payne, J.R., Reilly, T.J., French, D.P., 1999. Fabrication of a portable large-volume water sampling system to support oil spill NRDA efforts. Proc. 1999 Oil Spill Conf., Am. Petrol. Inst., Washington, D.C., 1179-1184.

Payne, J.R., Driskell, W.B., 2015a. 2010 DWH offshore water column samples—Forensic assessments and oil exposures. U.S. Dept. of Interior, Deepwater Horizon Response & Restoration, Admin. Record, www.doi.gov/deepwaterhorizon/adminrecord, DWH-AR0039118, 37 p.

Payne, J.R., Driskell, W.B., 2015b. Offshore adaptive sampling strategies. U.S. Dept. of Interior, Deepwater Horizon Response & Restoration, Admin. Record, www.doi.gov/deepwaterhorizon/adminrecord, DWH-AR0023786, 75 p.

Payne, J.R., Driskell, W.B., 2015c. Dispersant effects on waterborne oil profiles and behavior. U.S. Dept. of Interior, Deepwater Horizon Response & Restoration, Admin. Record, www.doi.gov/deepwaterhorizon/adminrecord, DWH-AR0039201, 22 p.

Prince, R. C., Elmendorf, D.L. Lute, J.R., Hsu, C.S., Haith, C.E., Senius, J.D., Dechert, G.J., Douglas, G.S., Butler, E.L.,1994. 17α(H),21β(H)-hopane as a conserved internal marker for estimating the biodegradation of crude oil. Environ. Sci. .Tech.. 28(1): 142-145.

Prince, R. C., Owens, E.H., Sergy, G.A., 2002. Weathering of an Arctic oil spill over 20 years: the BIOS experiment revisited. Marine Pollution Bulletin 44(11): 1236-1242.

Prince, R.C., McFarlin, K.M., Butler, J.D., Febbo, E.J., Wang, F.C.Y., Nedwed, T.J., 2013. The primary biodegradation of dispersed crude oil in the sea. Chemosphere 90: 521-526.

Radović, J.R., Aeppli, C., Nelson, R.K., Jimenez, N., Reddy, C.M., Bayona, J.M., Albaigés, J., 2014. Assessment of photochemical processes in marine oil spill fingerprinting. Mar. Poll. Bull. 79: 268-277.

Ramseur, J.L., 2010. Deepwater Horizon Oil Spill: The fate of the oil. Congressional. Research Service Report 7-5700, Dec. 16.

Ruddy, B.M., Huettel, M., Kostka, J.E., Lobodin, V.V., Bythell, B.J., McKenna, A.M., Aeppli, C., Reddy, C.M., Nelson, R.K., Marshall, A.G., Rodgers, R.P., 2014. Targeted petroleomics: Analytical investigation of Macondo well oil oxidation products from Pensacola Beach. Energy & Fuels, 28: 4043-4050.

Ryerson, T.B., Camilli, R., Kessler, J.D., Kujawinski, E.B., Reddy, C.M., Valentine, D.L., Atlas, E., Blake, D.R., de Gouw, J., Meinardi, S., Parrish, D.D., Peischl, J., Seewald, J.S., Warneke, C., 2012. Chemical data quantify *Deepwater Horizon* hydrocarbon flow rate and environmental distribution. Proc. Nat'l. Acad. Sci. 109(50): 20246-20253.

Simoneit, B. R. T. , 1986. Cyclic terpenoids of the geosphere. Biological Markers in the Sedimentary Record. R. B. Johns. Amsterdam, Elsevier: 43-59.

Socolofsky, S. A., Adams, E.E., Sherwood, C.R., 2011. Formation dynamics of subsurface hydrocarbon intrusions following the *Deepwater Horizon* blowout. Geophys. Res. Letters 38(L09602, doi:10.1029/2011GL047174): 6 p.

Socolofsky, S.A., Adams, E.E., Boufadel, M.C., Aman, Z.M., Johanse, O., Konkel, W.J., Lindo, D., Madsen, M.N., North, E.W., Paris, C.B., Rasumssen, D., Reed, M., Ronnigen, P., Sim, L.H., Uhrenholdt, T., Anderson, K.G., Cooper, C., Nedwed, T.J., 2015. Intercomparison of oil spill prediction models for accidental blowout scenarios with and without subsea chemical dispersant injection. Marine Poll. Bull. 96: 110-126.

Spier, C., Stringfellow, W.T., Hazen, T.C., Conrad, M., 2013. Distribution of hydrocarbons released during the 2010 MC252 oil spill in deep offshore waters. Environmental Pollution 173:224-230.

Stout, S.A. and C.R. German, in prep. Characterization and flux of marine oil snow settling to shallow sediments in the northern Gulf of Mexico during the *Deepwater Horizon* oil spill.

Stout, S.A., Payne, J.R., 2016. Chemical composition of floating and sunken *in situ* burn residues from the *Deepwater Horizon* oil spill. Mar. Pollut. Bull. 108: 186-202.

Stout, S.A., Payne, J.R., Emsbo-Mattingly, S.D., Baker, G., 2016. Weathering of field-collected floating and stranded Macondo oils during and shortly after the *Deepwater Horizon* oil spill. Mar. Pollut. Bull. 105: 7-22.

Stout, S.A., Payne, J.R., Ricker, R.W., Baker, G., Lewis, C. submitted. Macondo Oil in Deep-Sea Sediments: Part 2 – Occurrence and distinction from background and natural oil seeps. Mar. Pollut. Bull.

Valentine, D.L., Kessler, J.D., Redmond, M.C., Mendes, S.D., Heintz, M.B. et al., 2010. Propane respiration jump-starts microbial response to a deep oil spill. Science 330: 208-211.

Wang, Z., Fingas, M., Blenkinsopp, S., Sergy, G., Landriault, M., Sigouin, L., Foght, J., Semple, K., Westlake, D.W.S., 1998. Comparison of oil composition changes due to biodegradation and physical weathering in different oils. J. Chromotogr. A, 809: 89-107.

Wang, Z., Fingas, M., Owens, E.H., Sigouin, L., Brown, C.E., 2001. Long-term fate and persistence of the spilled Metula oil in a marine salt marsh environment. Degradation of petroleum biomarkers. J. Chrom. A. 926: 275-290.

White, H. K., Hsing, P.-Y., Cho, W., Shank, T.M., Cordes, E.E., Quattrini, A.M., Nelson, R.K., Camilli, R., Demopoulos, A.W.J., German, C.R., Brooks, J.M., Roberts, H.H., Shedd, W., Reddy, C.M., Fisher, C.R., 2012. Impact of the *Deepwater Horizon* oil spill on a deep-water coral community in the Gulf of Mexico. Proc. Nat'l. Acad. Sci. 109(50): 20303-20308.

Table 1: Inventory of deep-sea sediment samples from 729 cores collected in 2010/2011.

Study ID	Dates	Sediment
2010-2011 Surveys[a]		**2782**
HOS Davis Cruise 03[b]	Sept. 8-28, 2010	142
Pisces Cruise 06	Sept. 25-Oct. 4, 2010	13
Atlantis Cruise	Dec. 4-15, 2010	45
HOS Davis Cruise 05[c]	Dec. 4-18, 2010	190
HOS Sweetwater Cruise 01	Mar. 10-13, 2011	18
HOS Sweetwater Cruise 02	Mar. 23-Apr. 24, 2011	612
Sarah Bordelon Cruise 09	May 23-Jun. 13, 2011	456
HOS Sweetwater Cruise 04	Jul. 14-Aug. 7, 2011	366
HOS Sweetwater Cruise 6 Leg 1	Aug. 24-Sept. 2, 2011	168
Holiday Chouest Cruise 01	Aug. 25-Sept. 13, 2011	112
Holiday Chouest Cruise 02	Sept. 15-30, 2011	84
HOS Sweetwater Cruise 6 Leg 2	Sept. 29-Oct. 21, 2011	414
Holiday Chouest Cruise 03	Oct. 1-25, 2011	162

[a] 47 low resolution cores collected from Nancy Foster Cruises (Jul. 21-30, 2010, Aug. 1-10, 2010), Cape Hatteras Cruise (Sept. 20-Oct. 3, 2010, and Ron Brown Cruise (Oct. 16-Nov. 3, 2010) were excluded

[b] 4 low resolution cores (n=12 intervals) were excluded

[c] 1 low resolution core (n=3 intervals) was excluded

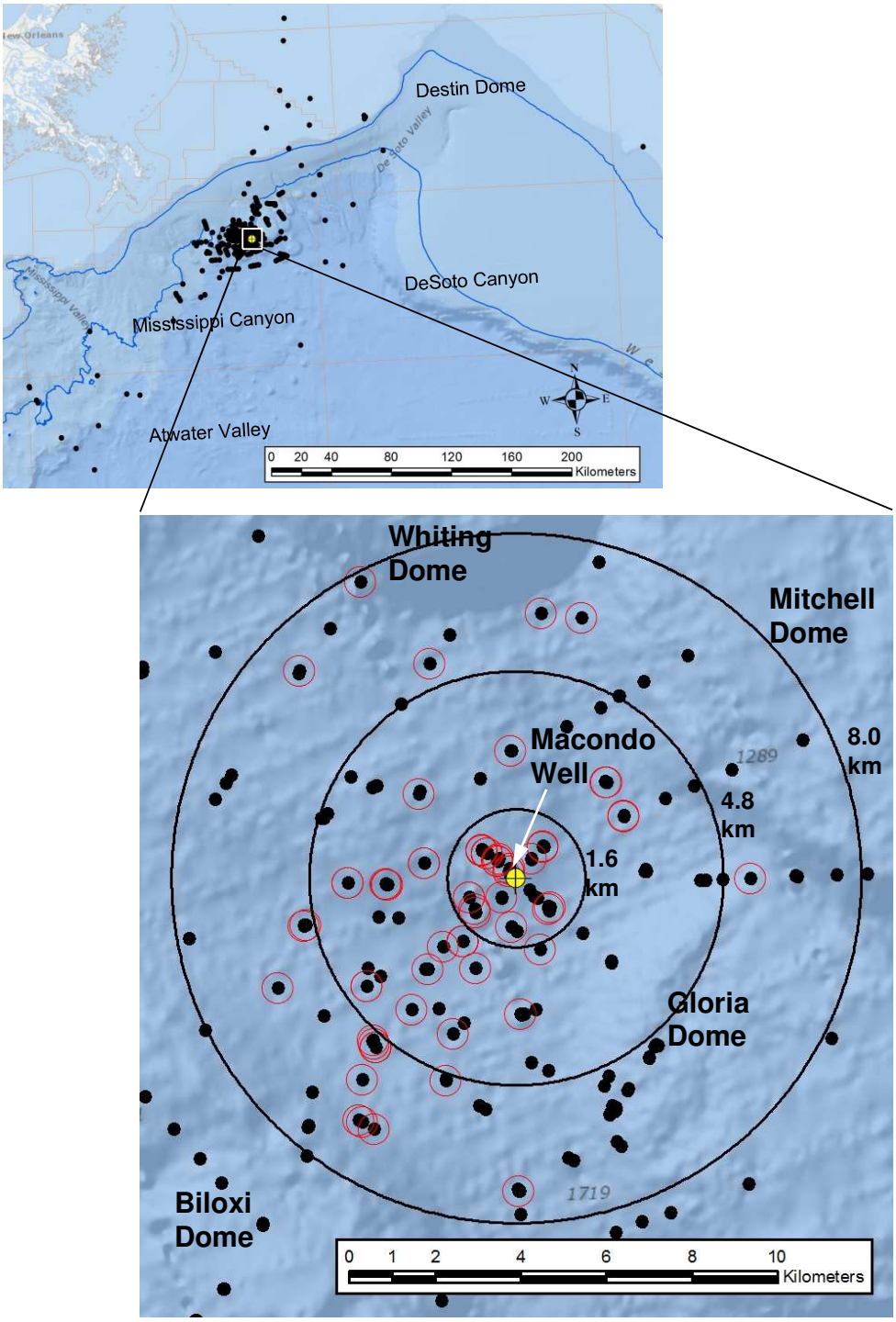

Figure 1: Maps showing the locations of 729 sediment cores collected in 2010/2011 considered (per Table 1). Top shows relevant BOEM lease regions and 200m and 1000m isobaths; bottom shows major topographic features and radii (1.6, 4.8, and 8.0 km) around the Macondo wellhead. Circled locations depict 69 cores containing a wax-rich, severely weathered oil described in detail herein (Table S-2). Note that many core locations actually represent up to 4 multi-cores collected within a few meters of one another.

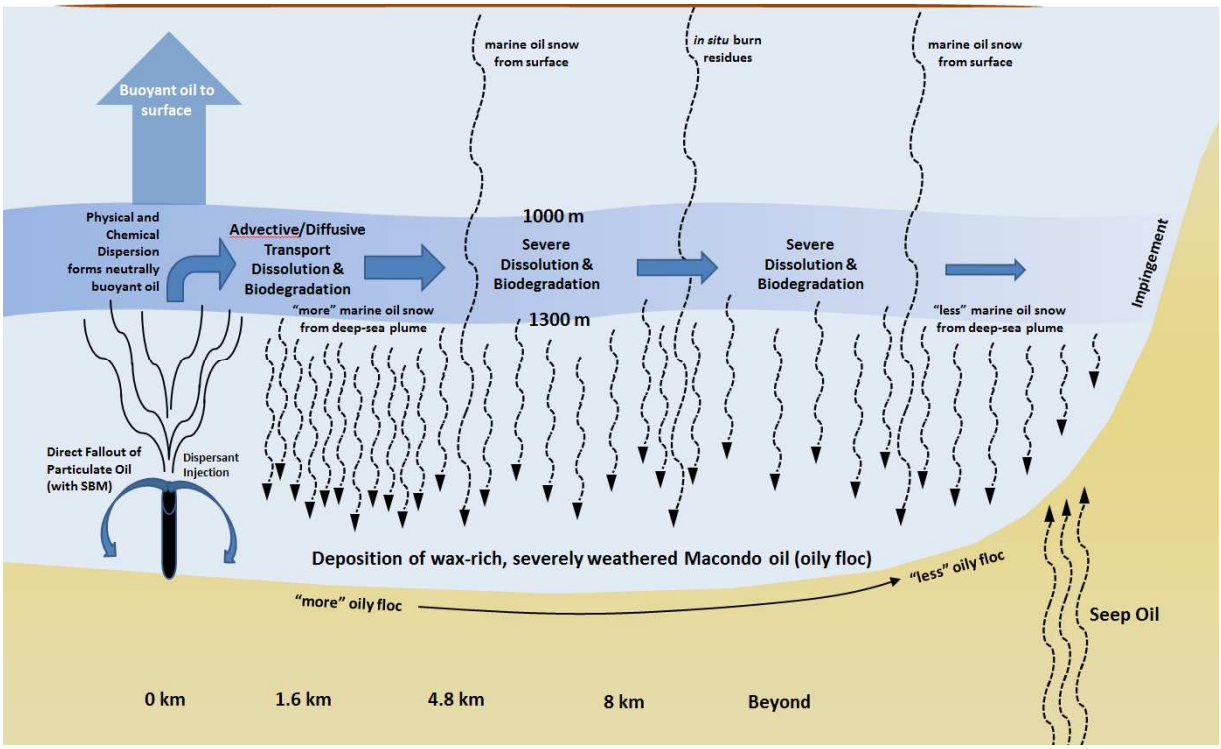

Figure 2: Conceptual model for Macondo oil deposition on the deep-sea floor.

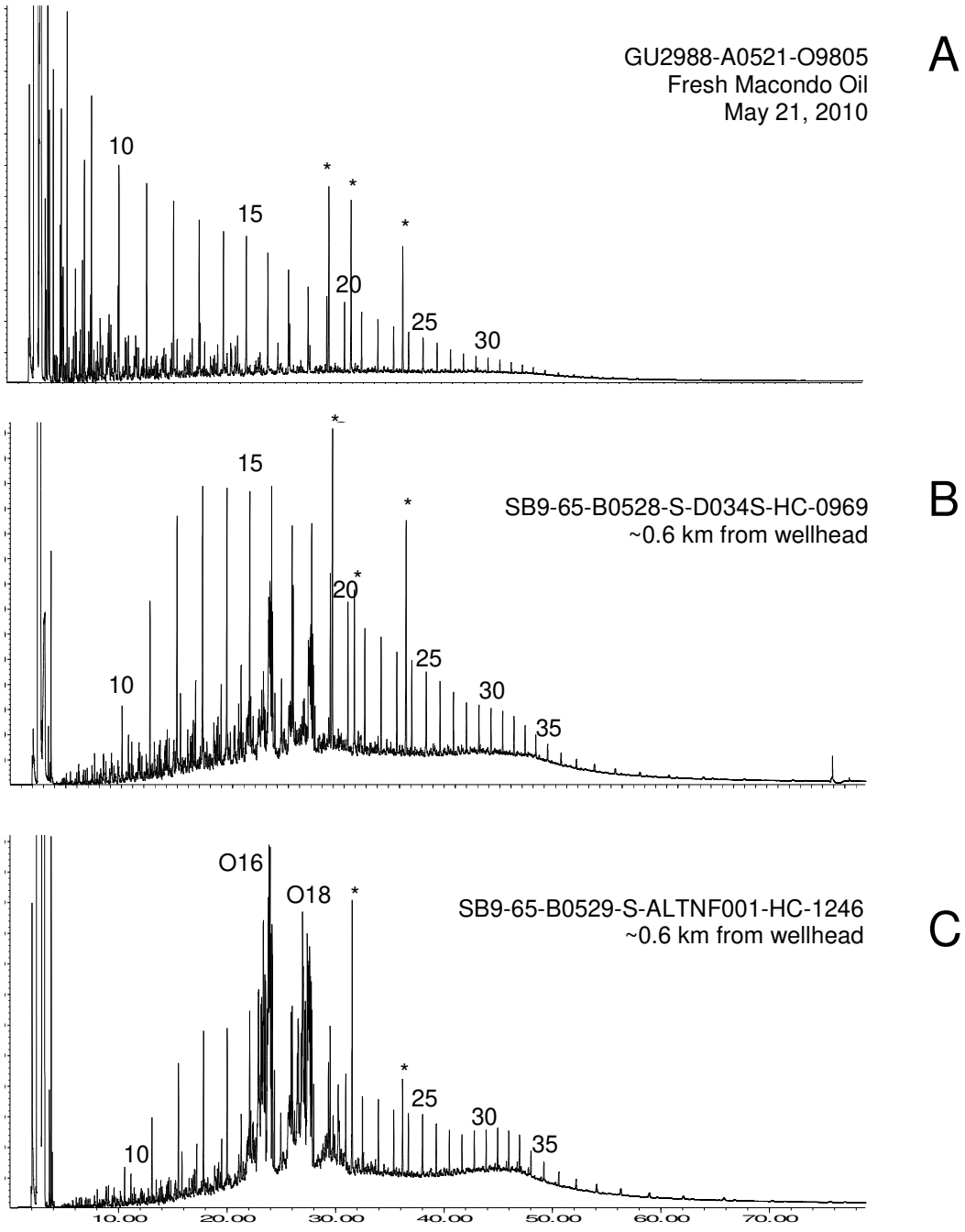

Figure 3: GC/FID chromatograms exemplifying the weathering and range of mixing (oil with synthetic based drilling mud) among surface (0-1 cm) sediments near the wellhead in May 2011. (A) fresh Macondo oil, (B) a sediment containing minimally weathered Macondo oil with minor synthetic-based mud, and (C) a sediment containing synthetic-based mud with a minor amount of a minimally weathered Macondo oil. # - n-alkane carbon number; O# - olefin cluster carbon number; * - internal standard.

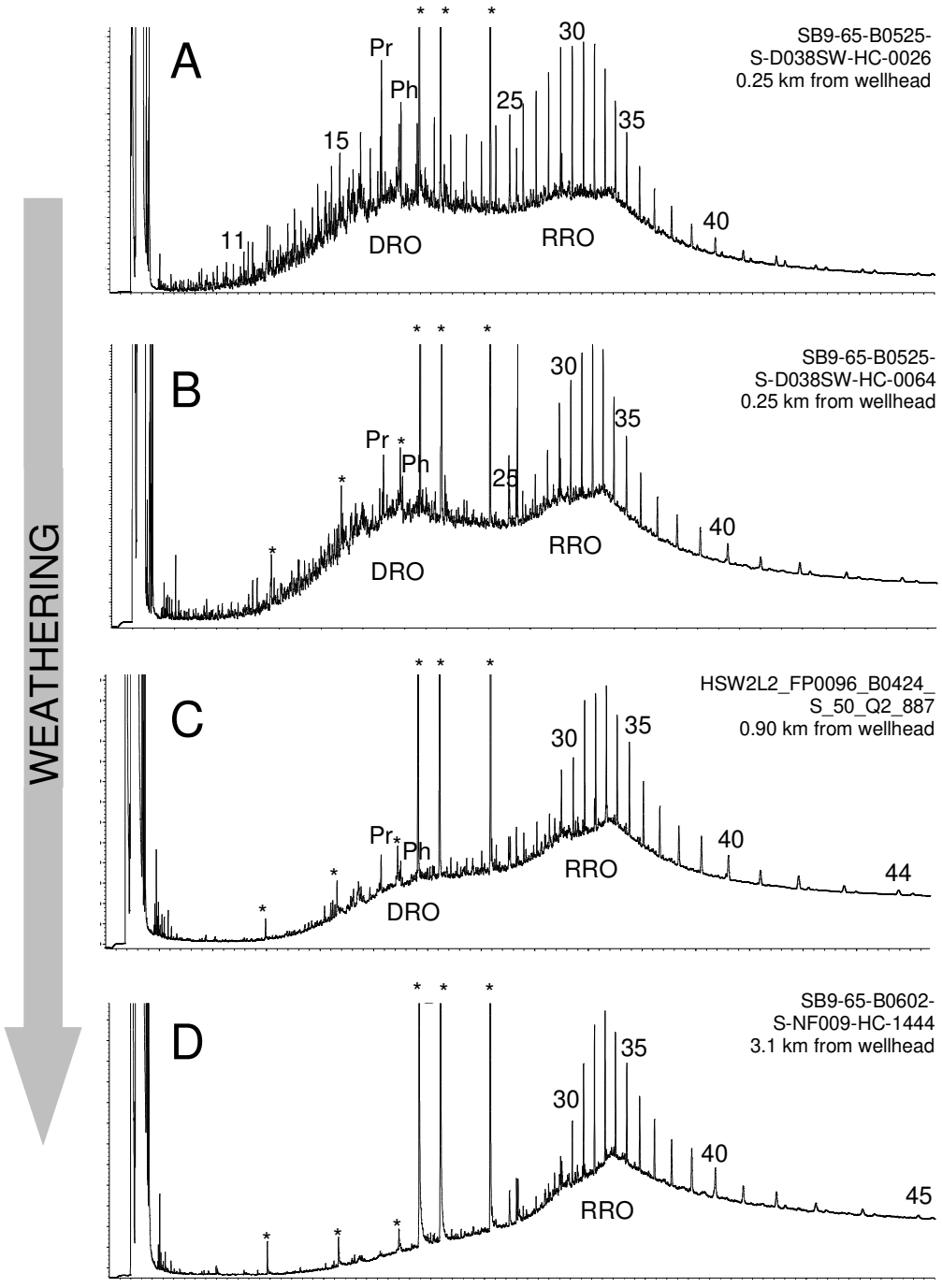

Figure 4: GC/FID chromatograms of surface sediments (0-1 cm) from four cores near the wellhead in 2011 that demonstrate the progression in weathering of Macondo oil. (A) partially weathered and wax-rich oil, (B) intermediately weathered and wax-rich oil, (C) highly weathered and wax-rich oil, and (D) severely weathered wax-rich oil Pr-pristane; Ph-phytane; # - n-alkane carbon number; * - internal standard. DRO – diesel range organics; RRO – residual range organics.

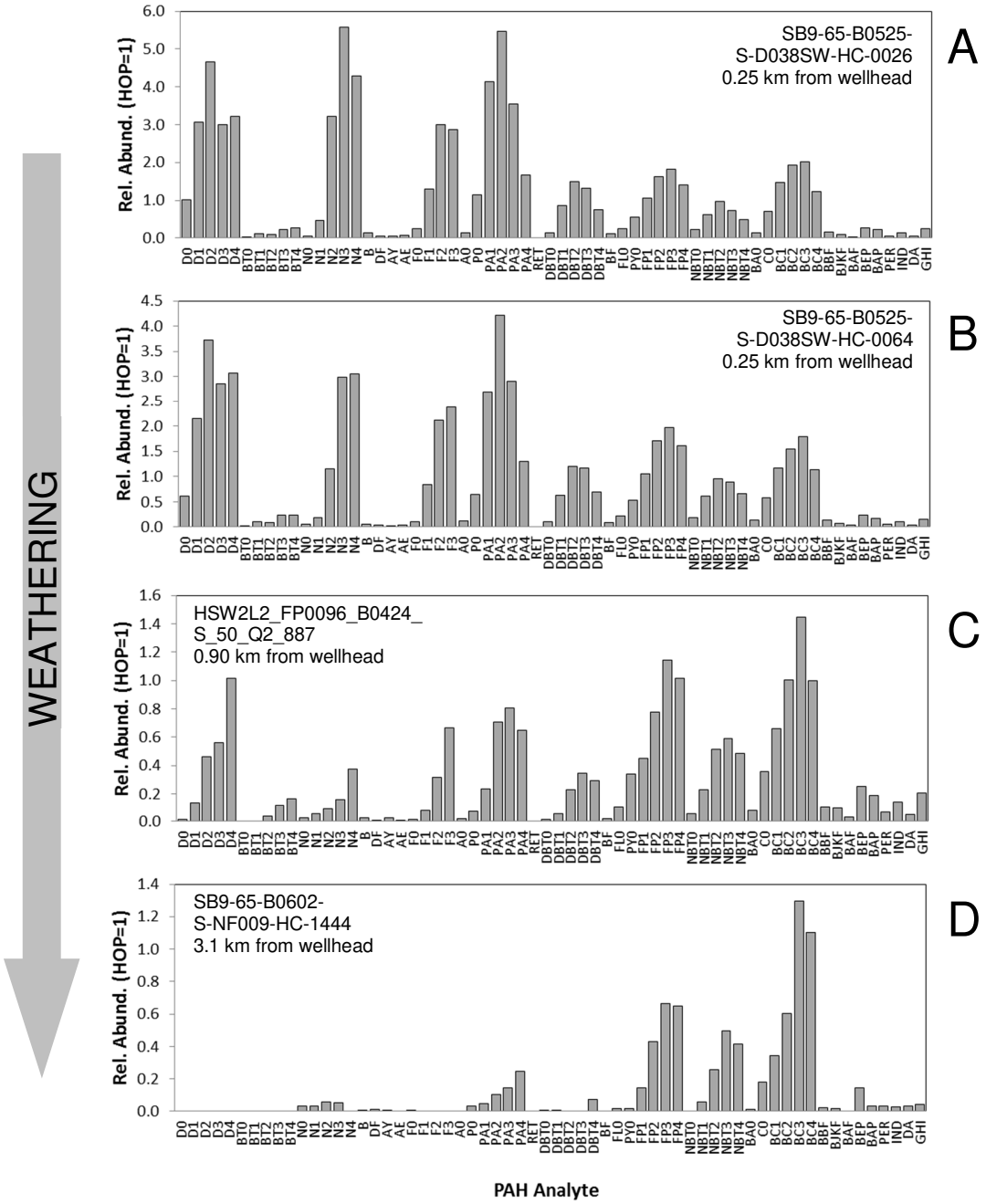

Figure 5: Histograms showing the hopane-normalized concentrations of PAH analytes in surface sediments (0-1 cm) from four cores near the wellhead in 2011 that demonstrate the progression in weathering of Macondo oil. (A) partially weathered and wax-rich oil, (B) intermediately weathered and wax-rich oil, (C) highly weathered and wax-rich oil, and (D) severely weathered wax-rich oil Same sample's GC/FID chromatograms are shown in Fig. 4. See Table S-1 for compound abbreviations.

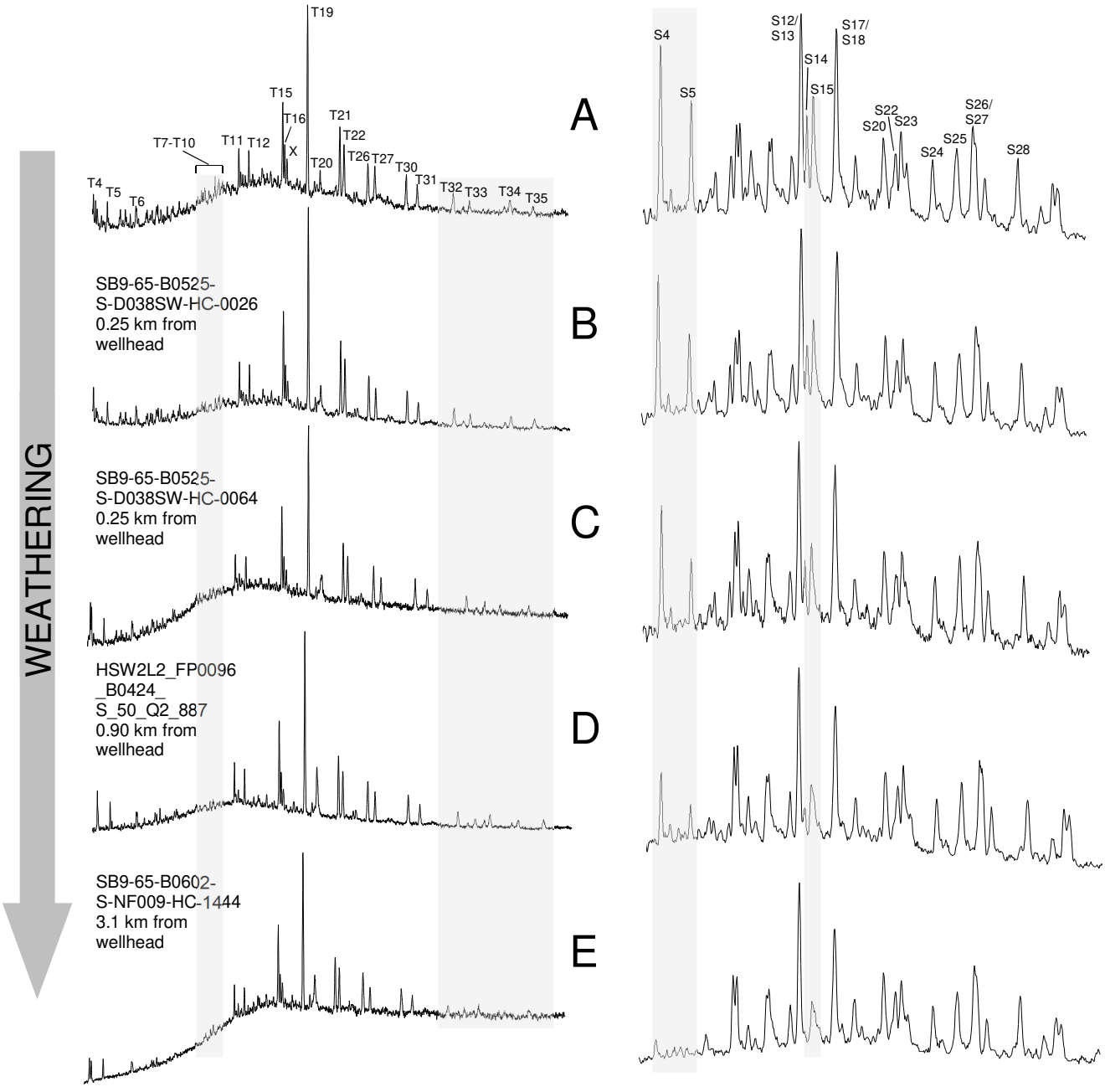

Figure 6: Partial extracted ion profiles showing the distributions of terpanes (*m/z* 191; left) and dia- and regular steranes (*m/z* 217; right) in fresh Macondo oil and surface sediments (0-1 cm) from four cores near the wellhead in 2011 that exemplify the range of weathering of Macondo oil. (A) fresh Macondo oil, (B) partially weathered and wax-rich oil, (C) intermediately weathered and wax-rich oil, (D) highly weathered and wax-rich oil, and (E) severely weathered wax-rich oil. Greyed regions highlight the progressive depletion of C_{28}-C_{29} tricyclic terpanes (T7-T10), C_{34}-C_{35} homohopanes (T32-T35), $\beta\alpha$-C_{27} diasteranes (S4 & S5) and $\beta\beta$-C_{27} steranes (S14 & S15). See Table S-1 for compound abbreviations.

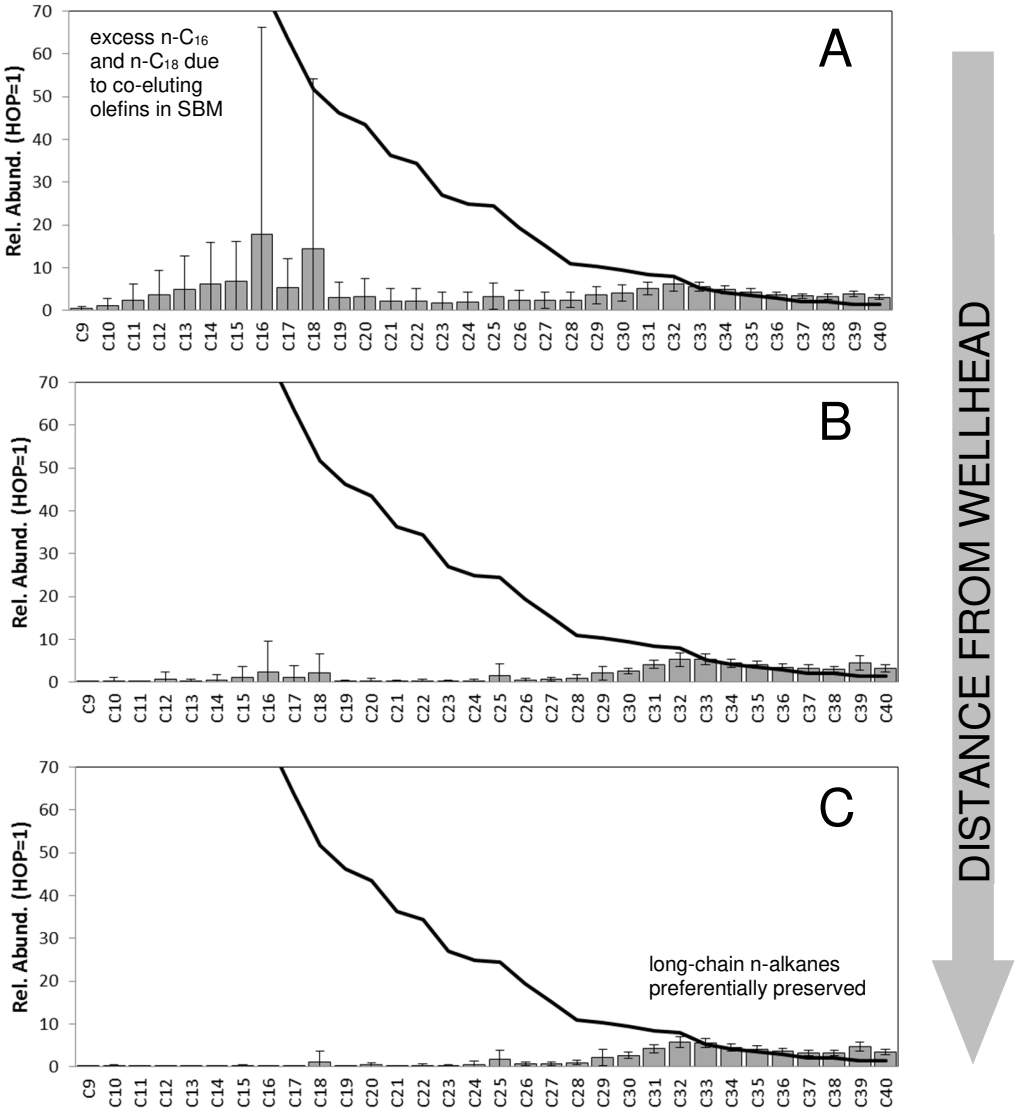

Figure 7: Histograms showing the hopane-normalized average concentrations of n-alkanes in severely weathered Macondo oil in surface sediments (0-1 cm) from 2010/2011: (A) 0 to 1.6 km from wellhead (n=23), (B) 1.6 to 4.8 km from wellhead (n=26), and (C) 4.8 to 8.0 km from wellhead (n=20). Solid line represents the average hopane-normalized concentrations of *n*-alkanes in fresh Macondo oil (Stout et al., 2016). Error bars = 1σ. Calculated from data in Table S-3. Compound abbreviations per Table S-1.

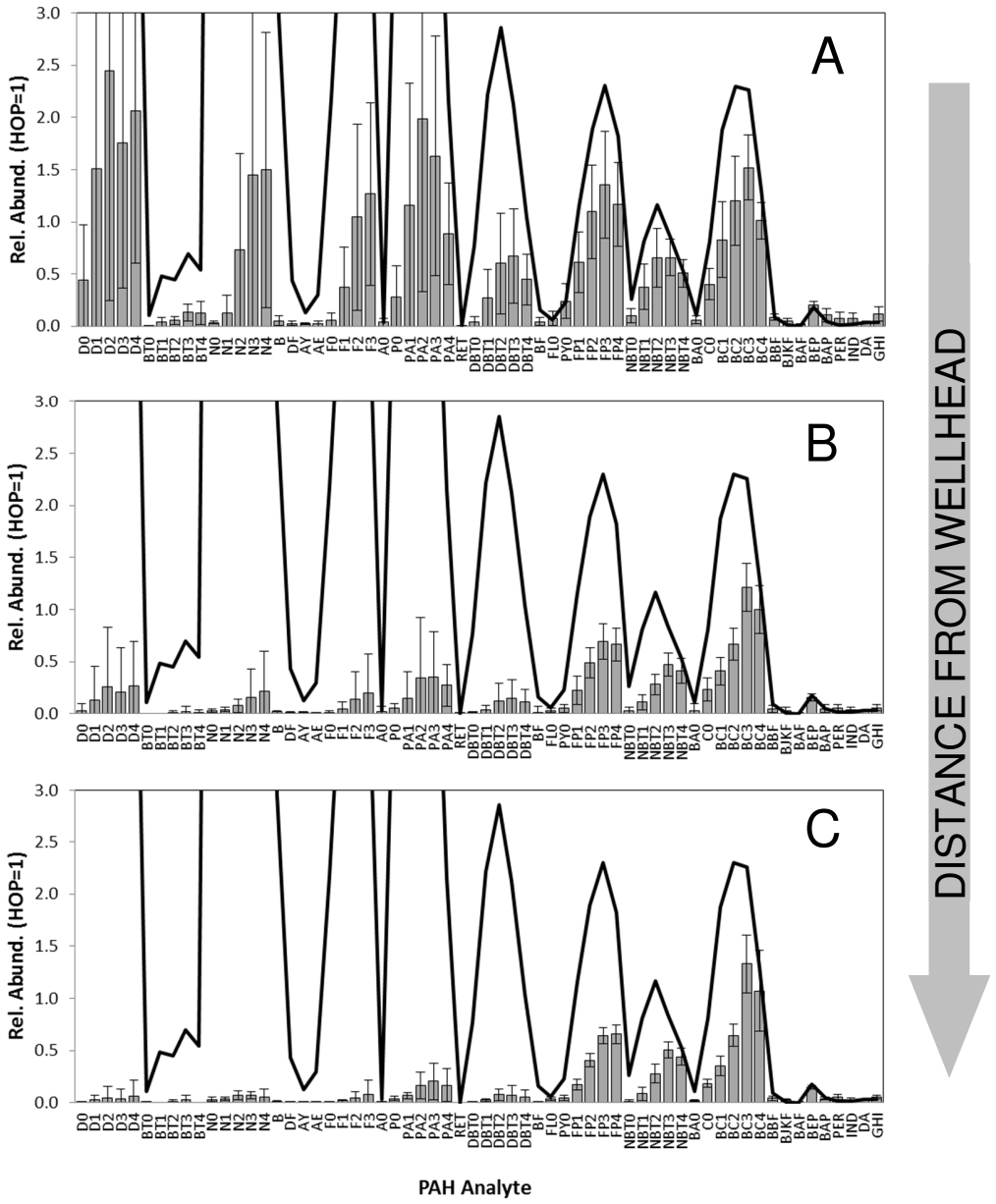

Figure 8: Histograms showing the average hopane-normalized concentrations of PAHs in severely weathered Macondo oil in surface sediments (0-1 cm) from 2010/2011: (A) 0 to 1.6 km from wellhead (n=23), (B) 1.6 to 4.8 km from wellhead (n=26), and (C) 4.8 to 8.0 km from wellhead (n=20). Solid line represents the average hopane-normalized concentrations of PAHs and other analytes in fresh Macondo oil (Stout et al., submitted). Error bars = 1σ. Calculated from data in Table S-4. Compound abbreviations per Table S-1.

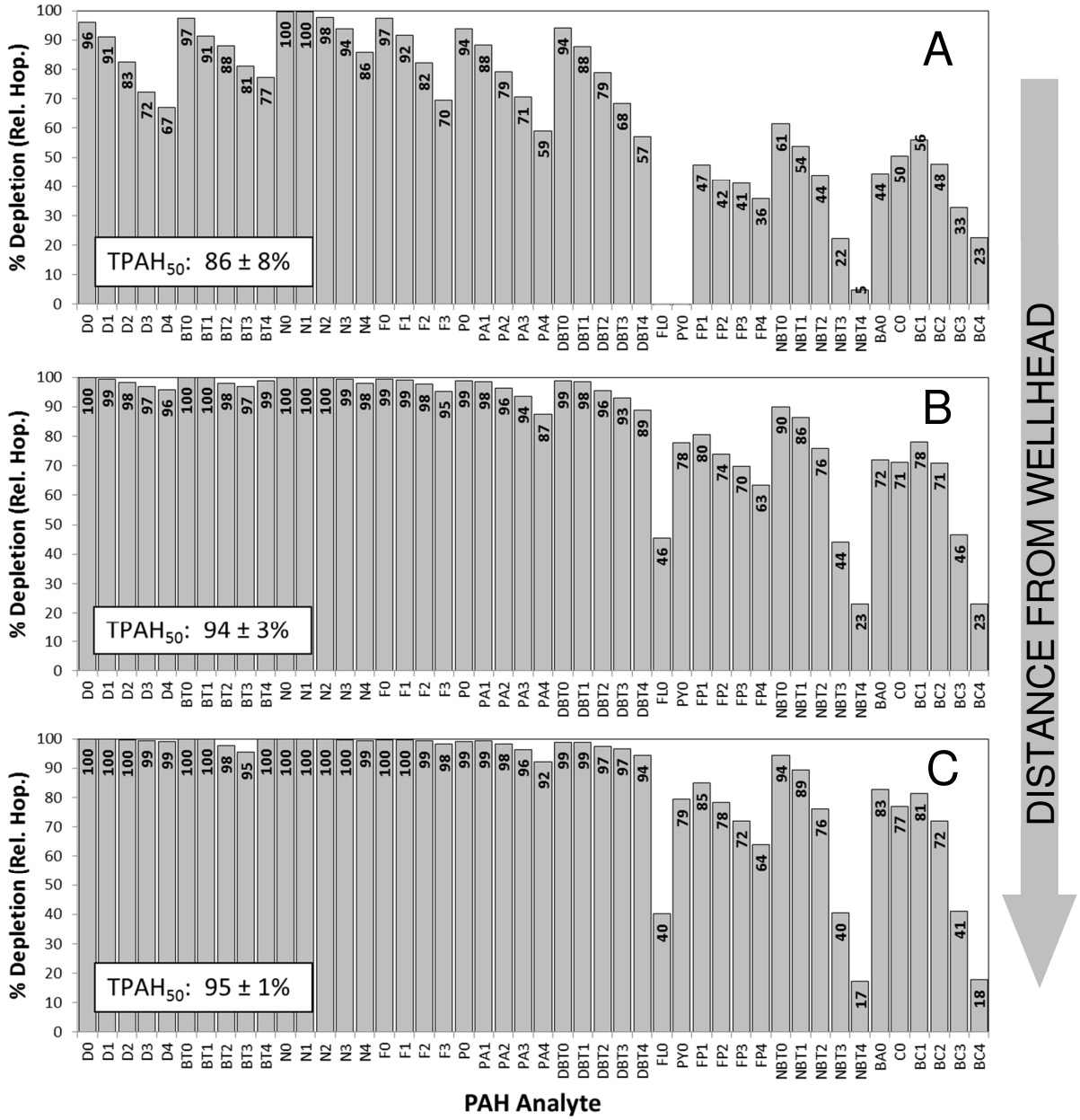

Figure 9: Histograms showing the average percent depletion of PAH homologue groups relative to hopane in severely weathered Macondo oil in surface sediments (0-1 cm) from 2010/2011: (A) 0 to 1.6 km from wellhead (n=23), (B) 1.6 to 4.8 km from wellhead (n=26), and (C) 4.8 to 8.0 km from wellhead (n=20). Individual and $TPAH_{50}$ percent depletions calculated per Eq. 1; using data from Table S-4). Compound abbreviations per Table S-1.

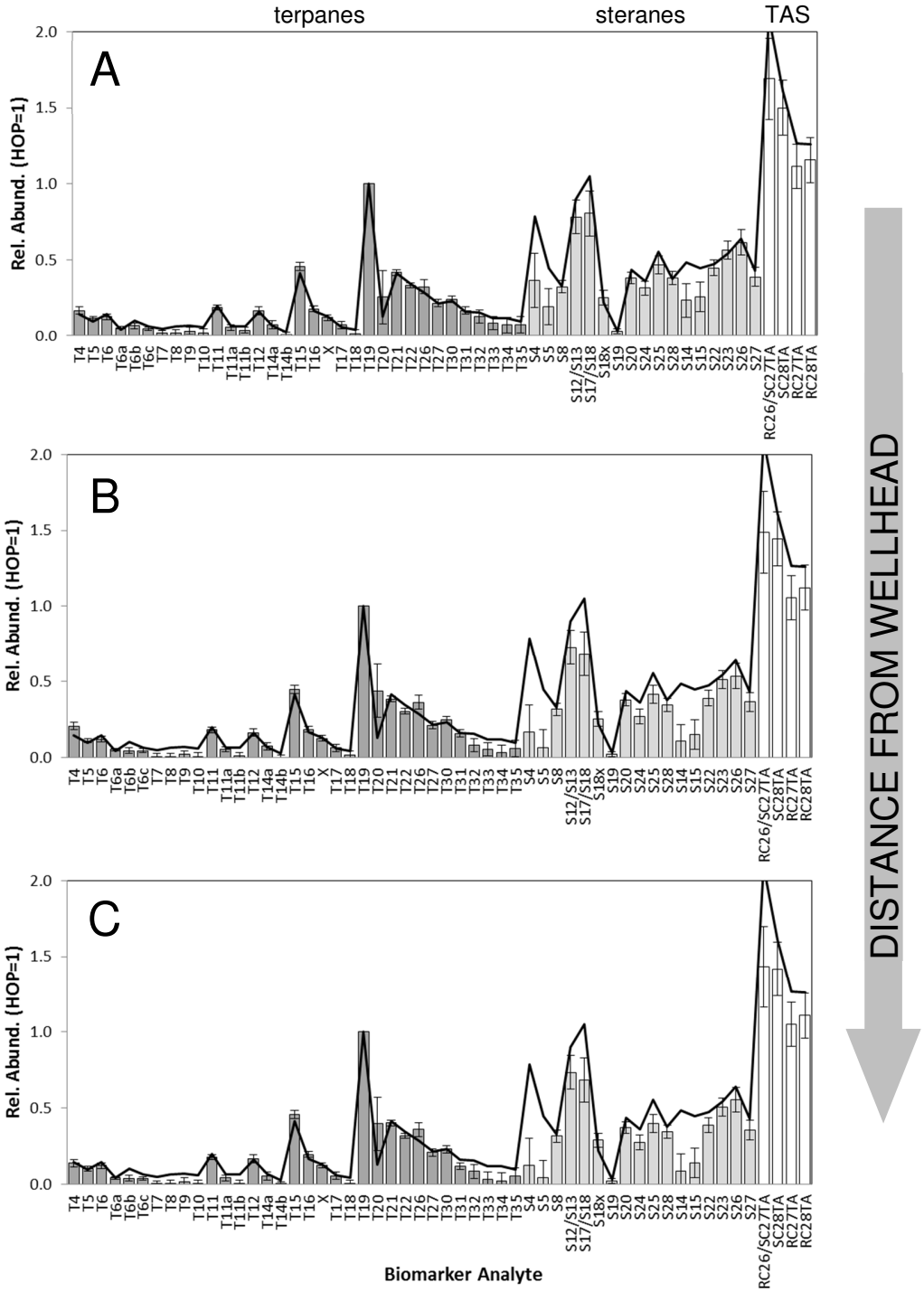

Figure 10: Histograms showing the average hopane-normalized concentrations of biomarkers in severely weathered Macondo oil in surface sediments (0-1 cm) from 2010/2011: (A) 0 to 1.6 km from wellhead (n=23), (B) 1.6 to 4.8 km from wellhead (n=26), and (C) 4.8 to 8.0 km from wellhead (n=20). Black line represents the average hopane-normalized concentrations of biomarkers in fresh Macondo oil (Stout et al., 2016). Error bars = 1σ. Calculated from data in Table S-5. Compound abbreviations per Table S-1.

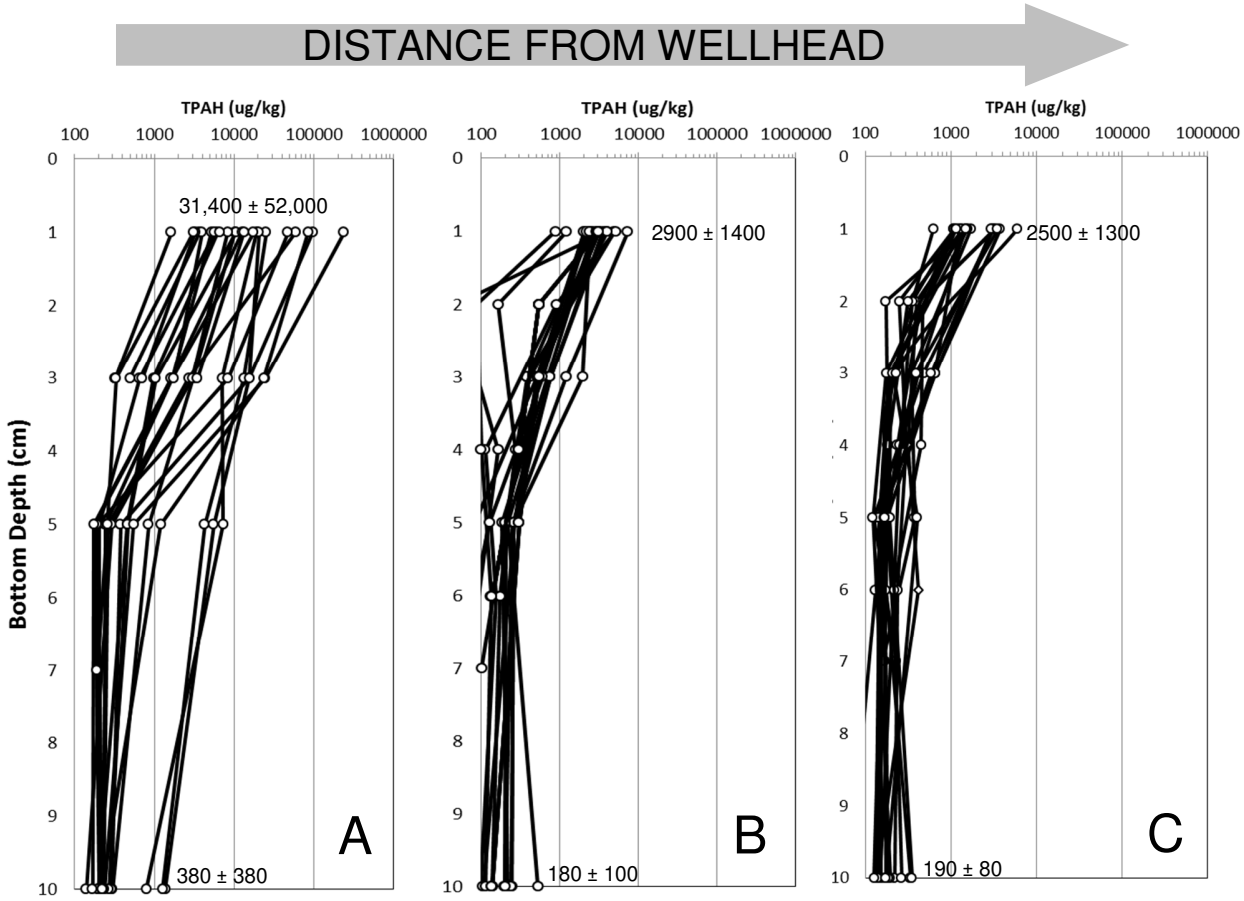

Figure 11: Graphs showing the concentrations of $TPAH_{50}$ in 2010/2011 cores containing wax-rich, severely weathered Macondo oil at the surface *versus* sediment depth for cores (A) 0 to 1.6 km (n=23), (B) 1.6 to 4.8 km (n=26), and (C) 4.8 to 8.0 km (n=20) from the well. Bottom depths of each interval are plotted on *y*-axes. $TPAH_{50}$ per Table S-1. $TPAH_{50}$ (µg/kg) average ± 1σ for 0-1 cm and 5-10 cm intervals are given.

Supporting Information

Macondo Oil in Deep-Sea Sediments: Part 1 – Sub-sea Weathering of Oil Deposited on the Seafloor

Scott A. Stout[1*] and James R. Payne[2]

[1]NewFields Environmental Forensics Practice, LLC, 300 Ledgewood Pl., Suite 305, Rockland, MA
[2]Payne Environmental Consultants, Inc. 1651 Linda Sue Ln., Encinitas, CA

6 Tables

Table S-1: Inventory of target analytes and abbreviations used in figures.

Abbrev.	Compound
C9	n-Nonane
C10	n-Decane
C11	n-Undecane
C12	n-Dodecane
C13	n-Tridecane
1380	2,6,10 Trimethyldodecane
C14	n-Tetradecane
1470	2,6,10 Trimethyltridecane
C15	n-Pentadecane
C16	n-Hexadecane
1650	Norpristane
C17	n-Heptadecane
Pr	Pristane
C18	n-Octadecane
Ph	Phytane
C19	n-Nonadecane
C20	n-Eicosane
C21	n-Heneicosane
C22	n-Docosane
C23	n-Tricosane
C24	n-Tetracosane
C25	n-Pentacosane
C26	n-Hexacosane
C27	n-Heptacosane
C28	n-Octacosane
C29	n-Nonacosane
C30	n-Triacontane
C31	n-Hentriacontane
C32	n-Dotriacontane
C33	n-Tritriacontane
C34	n-Tetratriacontane
C35	n-Pentatriacontane
C36	n-Hexatriacontane
C37	n-Heptatriacontane
C38	n-Octatriacontane
C39	n-Nonatriacontane
C40	n-Tetracontane
TPH	Total Petroleum Hydrocarbons

Abbrev.	Compound
D0	cis/trans-Decalin
D1	C1-Decalins
D2	C2-Decalins
D3	C3-Decalins
D4	C4-Decalins
BT0	Benzothiophene
BT1	C1-Benzo(b)thiophenes
BT2	C2-Benzo(b)thiophenes
BT3	C3-Benzo(b)thiophenes
BT4	C4-Benzo(b)thiophenes
N0	Naphthalene
N1	C1-Naphthalenes
N2	C2-Naphthalenes
N3	C3-Naphthalenes
N4	C4-Naphthalenes
B	Biphenyl
DF	Dibenzofuran
AY	Acenaphthylene
AE	Acenaphthene
F0	Fluorene
F1	C1-Fluorenes
F2	C2-Fluorenes
F3	C3-Fluorenes
A0	Anthracene
P0	Phenanthrene
PA1	C1-Phenanthrenes/Anthracenes
PA2	C2-Phenanthrenes/Anthracenes
PA3	C3-Phenanthrenes/Anthracenes
PA4	C4-Phenanthrenes/Anthracenes
RET	Retene
DBT0	Dibenzothiophene
DBT1	C1-Dibenzothiophenes
DBT2	C2-Dibenzothiophenes
DBT3	C3-Dibenzothiophenes
DBT4	C4-Dibenzothiophenes
BF	Benzo(b)fluorene
FL0	Fluoranthene
PY0	Pyrene
FP1	C1-Fluoranthenes/Pyrenes
FP2	C2-Fluoranthenes/Pyrenes
FP3	C3-Fluoranthenes/Pyrenes
FP4	C4-Fluoranthenes/Pyrenes
NBT0	Naphthobenzothiophenes
NBT1	C1-Naphthobenzothiophenes
NBT2	C2-Naphthobenzothiophenes
NBT3	C3-Naphthobenzothiophenes
NBT4	C4-Naphthobenzothiophenes
BA0	Benz[a]anthracene
C0	Chrysene/Triphenylene
BC1	C1-Chrysenes
BC2	C2-Chrysenes
BC3	C3-Chrysenes
BC4	C4-Chrysenes
BBF	Benzo[b]fluoranthene
BJKF	Benzo[jk]fluoranthene
BAF	Benzo[a]fluoranthene
BEP	Benzo[e]pyrene
BAP	Benzo[a]pyrene
PER	Perylene
IND	Indeno[1,2,3-cd]pyrene
DA	Dibenz[a,h]anthracene
GHI	Benzo[g,h,i]perylene

TPAH50 = Σ N0 to GHI, excluding RET and PER

Abbrev.	Compound
T4	C23 Tricyclic Terpane
T5	C24 Tricyclic Terpane
T6	C25 Tricyclic Terpane
T6a	C24 Tetracyclic Terpane
T6b	C26 Tricyclic Terpane-22S
T6c	C26 Tricyclic Terpane-22R
T7	C28 Tricyclic Terpane-22S
T8	C28 Tricyclic Terpane-22R
T9	C29 Tricyclic Terpane-22S
T10	C29 Tricyclic Terpane-22R
T11	18a(H)-22,29,30-Trisnorneohopane-T_S
T11a	C30 Tricyclic Terpane-22S
T11b	C30 Tricyclic Terpane-22R
T12	17a(H)-22,29,30-Trisnorhopane-T_M
T14a	17a/b & 21b/a 28,30-Bisnorhopane
T14b	17a(H),21b(H)-25-Norhopane
T15	17a(H),21b(H)-30-Norhopane
T16	18a(H)-30-Norneohopane-C29Ts
X	17a(H)-Diahopane
T17	17b(H),21a(H)-30-Normoretane
T18	18a(H)&18b(H)-Oleananes
T19	17a(H),21b(H)-Hopane
T20	17b(H),21a(H)-Moretane
T21	30-Homohopane-22S
T22	30-Homohopane-22R
T26	30,31-Bishomohopane-22S
T27	30,31-Bishomohopane-22R
T30	30,31-Trishomohopane-22S
T31	30,31-Trishomohopane-22R
T32	Tetrakishomohopane-22S
T33	Tetrakishomohopane-22R
T34	Pentakishomohopane-22S
T35	Pentakishomohopane-22R
S4	13b(H),17a(H)-20S-Diacholestane
S5	13b(H),17a(H)-20R-Diacholestane
S8	13b,17a-20S-Methyldiacholestane
S12/S13	14a(H),17a(H)-20S-Cholestane + 13b(H),17a(H)-20S-Ethyldiacholestane
S17/S18	14a(H),17a(H)-20R-Cholestane + 13b(H),17a(H)-20R-Ethyldiacholestane
S18x	Unknown sterane
S19	13a(H),17b(H)-20S-Ethyldiacholestane
S20	14a(H),17a(H)-20S-Methylcholestane
S24	14a(H),17a(H)-20R-Methylcholestane
S25	14a(H),17a(H)-20S-Ethylcholestane
S28	14a(H),17a(H)-20R-Ethylcholestane
S14	14b(H),17b(H)-20R-Cholestane
S15	14b(H),17b(H)-20S-Cholestane
S22	14b(H),17b(H)-20R-Methylcholestane
S23	14b(H),17b(H)-20S-Methylcholestane
S26	14b(H),17b(H)-20R-Ethylcholestane
S27	14b(H),17b(H)-20S-Ethylcholestane
RC26/ SC27TA	C26,20R- +C27,20S- triaromatic steroid
SC28TA	C28,20S-triaromatic steroid
RC27TA	C27,20R-triaromatic steroid
RC28TA	C28,20R-triaromatic steroid

Table S-2: Inventory of cores collected near the well containing wax-rich, severely weathered Macondo oil at relatively high concentrations as reflected by total PAH ($TPAH_{50}$) concentrations.

0 to 1.6 km (0 to 1 mile; n=23)	TPAH50 (0-1 cm; µg/kg)	1.6 to 4.8 km (1 to 3 miles; n=26)	TPAH50 (0-1 cm; µg/kg)	4.8 to 8.0 km (3 to 5 miles; n=20)	TPAH50 (0-1 cm; µg/kg)
SB9-65-B0528-S-D031S-HC-1087	238434	SB9-65-B0603-S-NF009-HC-1524	7242	HSW2_HSW2013_B0330_S_W5_A2_095	5984
SB9-65-B0525-S-D038SW-HC-0026	96364	HD5_HD5004_A1214_S_BR2_01	5114	HSW6_FP8204A_B0830_S_1357_50_M2_0313	4078
SB9-65-B0528-S-D031S-HC-1167	84683	HSW2L2_FP1091_B0423_S_50_O2_833	4928	SB9-65-B0607-S-D050S-HC-3097	3861
SB9-65-B0527-S-D040S-HC-0576	59188	HSW2L2_FP1091_B0423_S_50_M2_832	4019	HSW2L2_FP4077_B0418_S_50_O2_670	3758
SB9-65-B0529-S-ALTNF001-HC-1246	46947	HD5_HD5004_A1214_S_YW2_05	4013	HD5_HD5003_A1211_S_BL1_05	3271
SB9-65-B0525-S-D038SW-HC-0104	25111	SB9-65-B0603-S-NF011-HC-1718	3760	HSW2L2_FP5071B_B0417_S_50_I2_617	3152
SB9-65-B0526-S-D042S-HC-0222	22951	HSW2L2_FP2087_B0422_S_50_O2_797	3680	HSW2L2_FP5071_B0417_S_50_E2_612	2997
SB9-65-B0525-S-D042S-HC-0182	20373	SB9-65-B0603-S-NF012-HC-1798	3492	SB9-65-B0528-S-LBNL3-HC-0929	2971
SB9-65-B0525-S-D038SW-HC-0064	19135	HD5_HD5006_A1215_S_OR3_03	3286	HSW6_FP9200_B0830_S_1387_50_O2_0244	2957
SB9-65-B0526-S-NF006MOD-HC-0419	17620	SB9-65-B0603-S-NF010-HC-1564	3128	HSW2L2_BRP066_B0416_S_50_H2_575	2545
HSW2L2_FP0096_B0424_S_50_Q2_887	13239	HSW6_FP11192_B0828_S_1540_50_C2_0127	2908	HSW6_FP8206_B0831_S_1281_50_R2_0308	2255
SB9-65-B0602-S-LBNL1-HC-1404	12583	SB9-65-B0527-S-NF008-HC-0812	2640	SB9-65-B0527-S-LBNL14-HC-0692	1991
SB9-65-B0526-S-NF006MOD-HC-0458	10496	SB9-65-B0604-S-NF012-HC-1836	2490	HSW2L2_FP5071A_B0417_S_50_H2_616	1735
SB9-65-B0525-S-D042S-HC-0143	10261	SB9-65-B0602-S-NF009-HC-1444	2441	HSW2L2_FP4076_B0418_S_50_L2_662	1721
SB9-65-B0529-S-LBNL1-HC-1325	8302	HSW2L2_FP2084_B0422_S_50_F2_773	2369	SB9-65-B0605-S-D019S-HC-2428	1548
HSW2L2_FP0096_B0424_S_50_O2_886	6646	SB9-65-B0604-S-ALTNF015-HC-2230	2259	SB9-65-B0605-S-LBNL17-HC-2269	1482
SB9-65-B0526-S-D044S-HC-0301	6151	HSW2L2_FP2085_B0422_S_50_H2_780	2218	SB9-65-B0528-S-LBNL3-HC-0890	1309
SB9-65-B0526-S-D044S-HC-0340	5683	HSW6_FP11192_B0828_S_1540_50_A2_0125	2210	HSW2L2_FP4076_B0418_S_50_K2_661	1305
SB9-65-B0526-S-D044S-HC-0262	5183	HSW2L2_FP2087_B0422_S_50_Q2_799	2082	HSW2L2_FP4076_B0418_S_50_J2_660	1249
HSW2L2_FP1090_B0423_S_50_H2_824	3965	SB9-65-B0603-S-NF009-HC-1484	2072	SB9-65-B0527-S-LBNL14-HC-0615	623
HSW2L2_FP1090_B0423_S_50_K2_826	3253	HSW2L2_FP1088_B0423_S_50_A2_806	2043		
HSW2L2_FP0096_B0424_S_50_N2_885	3101	HD5_HD5008_A1217_S_BL2_01	1996		
HSW2L2_FP1089_B0423_S_50_G2_817	1635	HD5_HD5005_A1215_S_PU2_04	1541		
		HD5_HD5006_A1215_S_PU2_04	1428		
		HD5_HD5004_A1214_S_GR2_04	1217		
		HD5_HD5004_A1214_S_PU2_03	883		

Table S-3: Average and standard deviations of concentrations of n-alkanes, isoprenoids, and TPH in surface sediments (0-1 cm) from cores collected near the well containing wax-rich, severely weathered Macondo oil.

N-alkanes and isoprenoids	Fresh Macondo Oil*		0-1.6 km		1.6 to 4.8 km		4.8 to 8.0 km	
	Avg (n=6)	σ	Avg (n=23)	σ	Avg (n=26)	σ	Avg (n=20)	σ
n-Nonane (C9)	10080	1011	0.48	0.87	0.07	0.11	0.05	0.10
n-Decane (C10)	8867	784	1.30	2.14	0.35	0.78	0.19	0.38
n-Undecane (C11)	8509	610	2.82	4.39	0.13	0.16	0.17	0.21
n-Dodecane (C12)	7613	611	4.12	6.70	0.66	1.69	0.14	0.16
n-Tridecane (C13)	7022	831	5.39	8.49	0.23	0.43	0.11	0.10
2,6,10 Trimethyldodecane (1380)	1403	203	2.33	3.92	0.12	0.17	0.02	0.04
n-Tetradecane (C14)	6248	465	6.50	10.22	0.60	1.17	0.14	0.15
2,6,10 Trimethyltridecane (1470)	2265	210	3.96	6.00	0.31	0.51	0.08	0.11
n-Pentadecane (C15)	6312	486	7.77	12.45	1.12	2.55	0.20	0.23
n-Hexadecane (C16)	5231	385	19.35	50.12	2.49	7.15	0.14	0.22
Norpristane (1650)	1609	240	3.85	5.66	0.24	0.40	0.05	0.10
n-Heptadecane (C17)	4385	330	6.01	9.66	1.11	2.83	0.18	0.19
Pristane	2919	199	19.84	37.39	4.67	13.67	0.22	0.18
n-Octadecane (C18)	3565	269	15.41	40.82	2.17	4.48	1.25	2.40
Phytane	1568	122	14.61	40.36	0.91	1.91	0.21	0.21
n-Nonadecane (C19)	3190	359	3.19	4.58	0.16	0.35	0.11	0.28
n-Eicosane (C20)	2993	221	3.74	5.65	0.39	0.45	0.48	0.44
n-Heneicosane (C21)	2503	166	2.34	3.59	0.20	0.23	0.13	0.11
n-Docosane (C22)	2369	181	2.61	4.17	0.25	0.42	0.27	0.39
n-Tricosane (C23)	1859	126	1.96	3.01	0.31	0.29	0.30	0.20
n-Tetracosane (C24)	1710	115	2.25	3.47	0.39	0.35	0.57	0.74
n-Pentacosane (C25)	1692	169	3.60	5.46	1.63	2.62	1.77	2.07
n-Hexacosane (C26)	1334	97	2.67	3.91	0.56	0.45	0.72	0.51
n-Heptacosane (C27)	1043	81	2.61	3.61	0.76	0.42	0.78	0.43
n-Octacosane (C28)	761	75	2.90	4.53	0.99	0.85	1.01	0.55
n-Nonacosane (C29)	713	80	3.87	5.55	2.18	1.58	2.20	1.85
n-Triacontane (C30)	653	50	4.44	6.64	2.57	0.65	2.65	0.75
n-Hentriacontane (C31)	574	48	5.09	6.71	4.21	0.90	4.25	0.94
n-Dotriacontane (C32)	549	52	6.03	7.82	5.27	1.59	5.80	1.19
n-Tritriacontane (C33)	367	34	5.19	6.22	5.39	1.26	5.69	1.05
n-Tetratriacontane (C34)	297	35	4.45	5.30	4.45	0.96	4.55	0.76
n-Pentatriacontane (C35)	240	30	3.91	4.38	4.13	0.83	4.18	0.71
n-Hexatriacontane (C36)	209	21	3.31	3.99	3.52	0.75	3.59	0.77
n-Heptatriacontane (C37)	148	16	2.93	3.08	3.25	0.76	3.36	0.64
n-Octatriacontane (C38)	141	18	2.76	2.76	3.05	0.70	3.24	0.66
n-Nonatriacontane (C39)	108	15	2.99	2.53	4.48	1.66	4.70	1.01
n-Tetracontane (C40)	100	33	2.37	1.94	3.24	0.86	3.50	0.66
TPH (C9-C44)	681389	53454	4239	5857	571	311	368	322

*as reported by Stout et al. (2016)

all conc in μg/g oil (oil) or μg/kg dry (sed)

Table S-4: Average and standard deviations of concentrations of decalins, PAHs and sulfur-containing aromatics in surface sediments (0-1 cm) from cores collected near the well containing wax-rich, severely weathered Macondo oil.

PAH and Related Compounds	Fresh Macondo Oil*		0-1.6 km		1.6 to 4.8 km		4.8 to 8.0 km	
	Avg (n=6)	σ	Avg (n=23)	σ	Avg (n=26)	σ	Avg (n=20)	σ
cis/trans-Decalin	779	43	689	1500	5	10	0.7	1.4
C1-Decalins	1174	56	2191	4614	26	46	10	18
C2-Decalins	966	36	3168	6097	54	84	18	47
C3-Decalins	436	13	2140	3875	42	68	15	39
C4-Decalins	431	29	2457	4291	67	88	25	66
Benzothiophene	7.3	0.6	3.3	6.0	nd	nd	0	0
C1-Benzo(b)thiophenes	33	1.2	50	88	nd	nd	nd	nd
C2-Benzo(b)thiophenes	31	1.9	58	92	2.3	4.0	3.4	4.1
C3-Benzo(b)thiophenes	48	3.8	151	257	5.5	12	10	14
C4-Benzo(b)thiophenes	37	0.4	164	303	0.8	3.9	nd	nd
Naphthalene	964	68	35	58	8.7	4.3	7.5	2.8
C1-Naphthalenes	2106	123	130	205	12	7.1	9.3	4.2
C2-Naphthalenes	2259	297	952	1852	21	13	17	9
C3-Naphthalenes	1597	63	1942	3806	34	39	18	11
C4-Naphthalenes	721	25	1886	3437	48	60	21	30
Biphenyl	204	20	52	71	4.7	2.5	3.8	2.1
Dibenzofuran	30	2.8	28	40	2.3	1.2	2.3	1.5
Acenaphthylene	8.9	1.1	22	34	2.9	1.4	2.4	1.1
Acenaphthene	21	4.4	25	54	0.5	1.6	0.1	0.3
Fluorene	150	12	71	131	3.5	2.5	2.4	1.5
C1-Fluorenes	308	27	486	899	11	11	5.4	4.1
C2-Fluorenes	404	24	1305	2350	33	43	16	25
C3-Fluorenes	286	19	1495	2571	42	66	29	59
Anthracene	2.3	6.3	43	75	4.3	15	1.2	1.1
Phenanthrene	310	32	340	627	14	11	10	3
C1-Phenanthrenes/Anthracenes	676	54	1570	3102	35	40	20	14
C2-Phenanthrenes/Anthracenes	657	45	2568	4817	79	92	52	56
C3-Phenanthrenes/Anthracenes	381	19	2039	3748	88	75	67	74
C4-Phenanthrenes/Anthracenes	148	12	1031	1766	79	55	60	62
Retene	nd	nd	0.8	3.9	0.3	1.4	nd	nd
Dibenzothiophene	53	6.8	54	91	2.7	1.8	2.3	1.2
C1-Dibenzothiophenes	153	16	378	743	8.8	8.1	7.8	5.9
C2-Dibenzothiophenes	197	18	776	1432	31	28	24	24
C3-Dibenzothiophenes	146	14	818	1432	37	34	26	39
C4-Dibenzothiophenes	72	5.2	514	861	31	23	22	26
Benzo(b)fluorene	11	1.0	54	93	3.7	16	0.6	1.1
Fluoranthene	4.1	1.1	57	79	8.4	3.5	8.8	3.0
Pyrene	16	3.2	207	241	13	8.3	13	10
C1-Fluoranthenes/Pyrenes	80	5.6	622	896	64	38	52	30
C2-Fluoranthenes/Pyrenes	130	9.1	1141	1692	147	72	121	61
C3-Fluoranthenes/Pyrenes	158	11	1424	2115	212	105	189	87
C4-Fluoranthenes/Pyrenes	125	8.9	1209	1739	206	109	192	89
Naphthobenzothiophenes	18	1.9	122	209	6.8	8.4	4.6	5.5
C1-Naphthobenzothiophenes	56	5.8	436	721	31	18	27	25
C2-Naphthobenzothiophenes	80	7.0	716	1104	83	39	83	49
C3-Naphthobenzothiophenes	58	4.9	645	861	148	77	144	61
C4-Naphthobenzothiophenes	37	7.0	485	621	128	70	126	54
Benz[a]anthracene	7.3	1.6	53	65	7.9	18	4.8	2.6
Chrysene/Triphenylene	56	5.4	424	636	69	43	56	31
C1-Chrysenes	129	11	926	1516	123	69	106	61
C2-Chrysenes	158	16	1303	2049	206	116	190	89
C3-Chrysenes	156	18	1492	2107	378	206	375	150
C4-Chrysenes	90	12	952	1268	314	176	314	147
Benzo[b]fluoranthene	6.1	0.9	75	87	13	10	11	5.7
Benzo[jk]fluoranthene	0.5	1.0	31	33	8.2	10	6.7	3.9
Benzo[a]fluoranthene	nd	nd	8.8	11	1.5	2.8	0.5	1.6
Benzo[e]pyrene	12	1.2	174	191	49	28	44	20
Benzo[a]pyrene	3.2	0.8	78	77	14	12	11	6.1
Perylene	1.0	0.3	46	34	14	5.6	13	2.7
Indeno[1,2,3-cd]pyrene	1.2	0.7	50	46	10	7.1	8.6	3.9
Dibenz[a,h]anthracene	2.5	0.8	34	39	9.2	5.4	8.1	3.6
Benzo[g,h,i]perylene	2.3	0.8	81	78	17	10	15	6.2
Σ N0-GHI, excl. RET & PER	13300	507	31400	52000	2900	1400	2500	1300

*as reported by Stout et al. (2016)

all conc in µg/g oil (oil) or µg/kg dry (sed)

Table S-5: Average and standard deviations of concentrations of biomarkers in surface sediments (0-1 cm) from cores collected near the well containing wax-rich, severely weathered Macondo oil.

PAH and Related Compounds	Fresh Macondo Oil*		0-1.6 km		1.6 to 4.8 km		4.8 to 8.0 km	
	Avg (n=6)	σ	Avg (n=23)	σ	Avg (n=26)	σ	Avg (n=20)	σ
Hopane	69	4.8	870	998	320	185	294	130
C23 Tricyclic Terpane	10	1.4	136	137	59	45	41	19
C24 Tricyclic Terpane	7	0.8	95	97	35	19	30	14
C25 Tricyclic Terpane	10	1.3	112	137	37	18	35	16
C24 Tetracyclic Terpane	3.0	0.3	45	46	17	11	13	8.6
C26 Tricyclic Terpane-22S	7.0	0.7	67	89	14	8.3	12	8.0
C26 Tricyclic Terpane-22R	4.6	0.6	45	63	13	7.6	12	7.6
C28 Tricyclic Terpane-22S	3.3	0.5	25	46	1.5	4.1	1.0	2.5
C28 Tricyclic Terpane-22R	4.3	0.5	26	41	2.0	6.4	2.0	5.7
C29 Tricyclic Terpane-22S	4.8	0.4	41	68	6.1	9.0	6.2	8.3
C29 Tricyclic Terpane-22R	4.1	0.5	32	58	1.6	4.0	1.8	4.3
18a-22,29,30-Trisnorneohopane-TS	14	1.2	165	190	58	34	52	25
C30 Tricyclic Terpane-22S	4.3	0.7	50	57	14	10	10	8.4
C30 Tricyclic Terpane-22R	4.4	0.8	37	40	3.2	5.8	2.4	6.0
17a(H)-22,29,30-Trisnorhopane-TM	11	1.0	140	147	52	28	48	22
17a/b,21b/a 28,30-Bisnorhopane	4.9	0.9	70	84	24	20	19	18
17a(H),21b(H)-25-Norhopane	1.7	1.4	18	42	nd	nd	0.3	1.5
30-Norhopane	29	2.7	395	454	142	79	133	60
18a(H)-30-Norneohopane-C29Ts	11	1.3	150	163	58	32	56	24
17a(H)-Diahopane	8.8	1.3	102	110	40	22	37	17
30-Normoretane	4.2	2.3	61	52	21	17	19	16
18a(H)&18b(H)-Oleananes	3.0	0.6	22	36	5.9	10	2.0	5.4
Moretane	8.8	1.0	159	113	128	74	106	81
30-Homohopane-22S	29	2.5	356	395	123	71	117	51
30-Homohopane-22R	24	2.1	289	325	95	51	91	38
30,31-Bishomohopane-22S	20	1.3	268	290	110	54	101	39
30,31-Bishomohopane-22R	15	1.2	187	228	67	36	62	28
30,31-Trishomohopane-22S	16	1.2	204	216	77	40	70	34
30,31-Trishomohopane-22R	11	1.1	145	177	50	29	37	26
Tetrakishomohopane-22S	11	1.3	122	152	26	25	28	23
Tetrakishomohopane-22R	7.9	1.6	86	111	18	19	13	17
Pentakishomohopane-22S	8.0	1.5	82	124	11	15	9	14
Pentakishomohopane-22R	6.8	0.8	78	98	17	21	17	21
13b(H),17a(H)-20S-Diacholestane	54	3.6	407	634	47	22	39	26
13b(H),17a(H)-20R-Diacholestane	31	2.8	232	392	18	13	15	16
13b,17a-20S-Methyldiacholestane	23	2.3	294	357	101	58	93	45
14a(H),17a(H)-20S-Cholestane + 13b(H),17a(H)-20S-Ethyldiacholestane	62	5.4	730	899	234	137	216	98
14a(H),17a(H)-20R-Cholestane + 13b(H),17a(H)-20R-Ethyldiacholestane	72	5.3	764	964	220	132	204	99
Unknown sterane	15	2.1	216	250	80	47	86	49
13a,17b-20S-Ethyldiacholestane	2.1	0.8	29	37	6.7	6.0	6.2	5.3
14a,17a-20S-Methylcholestane	30	0.8	342	410	124	77	108	48
14a,17a-20R-Methylcholestane	25	0.8	294	373	86	49	81	41
14a(H),17a(H)-20S-Ethylcholestane	38	6.1	429	523	135	80	119	60
14a(H),17a(H)-20R-Ethylcholestane	26	2.2	347	420	112	66	103	51
14b(H),17b(H)-20R-Cholestane	33	1.1	254	377	29	13	27	18
14b(H),17b(H)-20S-Cholestane	31	2.2	272	393	44	20	42	24
14b,17b-20R-Methylcholestane	32	2.3	403	466	127	80	116	58
14b,17b-20S-Methylcholestane	37	3.6	499	572	167	102	153	75
14b(H),17b(H)-20R-Ethylcholestane	44	3.8	550	623	173	104	166	79
14b(H),17b(H)-20S-Ethylcholestane	30	2.9	349	412	119	74	105	51
C26,20R- +C27,20S- triaromatic steroid	144	9.4	1533	1789	472	266	426	223
C28,20S-triaromatic steroid	111	5.8	1312	1435	461	266	421	225
C27,20R-triaromatic steroid	87	4.9	985	1123	335	188	310	158
C28,20R-triaromatic steroid	87	4.6	1000	1081	358	205	329	173

*as reported by Stout et al. (2016)

all conc in μg/g oil (oil) or μg/kg dry (sed)

Table S-6: Top: Average percent depletion of triaromatic steroids (TAS; relative to hopane) in surface sediments (0-1 cm) from cores collected near the well containing wax-rich, severely weathered Macondo oil. Middle: Selected physical properties of TAS. Bottom: Partial *m/z* 231 extracted ion profile showing the distribution of TAS in fresh Macondo oil.

TAS Congener(s)	Abbrev	Average Percent Depletion in Sediments		
		0 to 1.6 km (n=23)	1.6 to 4.8 km (n=26)	4.8 to 8.0 km (n=20)
C26 (20R) and C27 (20S)	RC26/SC27TA	19	29	32
C28 (20S)	SC28TA	7	10	12
C27 (20R)	RC27TA	12	17	17
C28 (20R)	RC28TA	8	11	12

Physical Properties of C_{26}-C_{28} TAS[a]	Mol. Wt. (g/mol)	Aqueous Solubility (mg/L)	log K_{ow} (mol/L)
C26 (20R and 20S)	344.5	5.37×10^{-6}	9.67
C27 (20R and 20S)	358.6	3.24×10^{-6}	9.87
C28 (20R and 20S)	372.6	1.19×10^{-6}	10.26

[a] per Aeppli et al. 2014; as calculated by SPARC on-line calculator; http://archemcalc.com/sparc

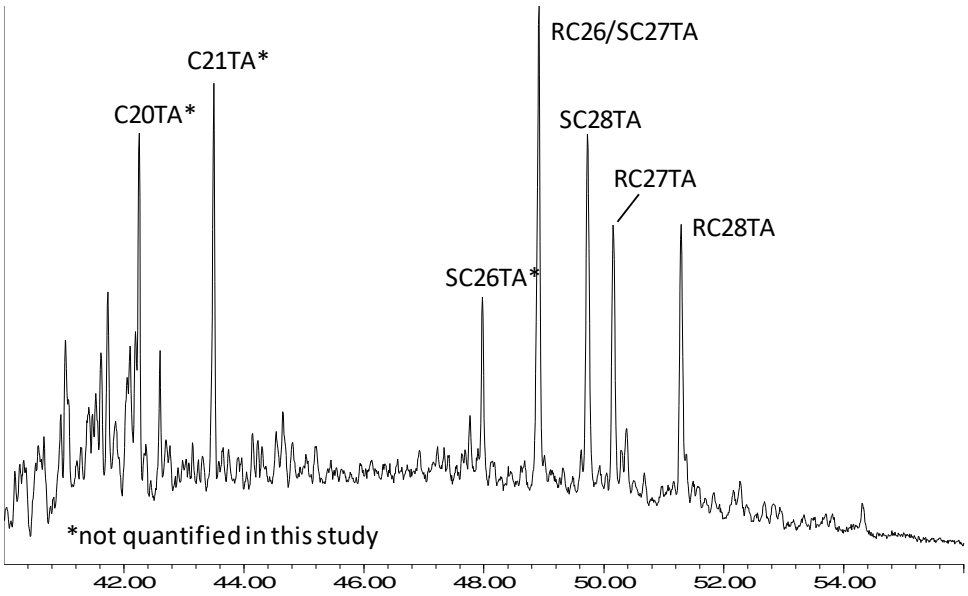

C_{26} to C_{28} Triaromatic Steroids in Fresh Macondo Oil (*m/z* 231)